Combining basin modelling with high-resolution heat-flux simulations to investigate the key drivers for burial dolomitisation in an offshore carbonate reservoir

Combining basin modelling with high-resolution heat-flux simulations to investigate the key drivers for burial dolomitisation in an offshore carbonate reservoir

A. Mangione [1,2], H. Lewis [1,2], S. Geiger [1,2], R. Wood [2,3], S. Beavington-Penney [4], J. McQuilken [5] & J. Cortes [6]*

1. Institute of Petroleum Engineering, Heriot-Watt University (Riccarton, Edinburgh, EH14 4AS, UK),
2. International Centre for Carbonate Reservoir (ICCR)
3. School of Geosciences, University of Edinburgh (Grant Institute, University of Edinburgh, Kings Buildings, West Mains Road, Edinburgh EH9 3JW, U.K.),
4. School of Earth and Ocean Sciences, Cardiff University, Main Building (Park Place, Cardiff, CF10 3AT)
5. BG Group (Thames Valley Park, Reading, RG6 1PT,UK),
6. Glencore E&P (50 Berkeley Street, London, W1J 8HD)

***Corresponding author (e-mail: am828@hw.ac.uk)**

ABSTRACT

The Eocene El Garia Formation in the offshore Hasdrubal Field was originally a nummulitic limestone in which subsequent burial dolomitisation has significantly enhanced permeability. Identification of the reservoir's petrophysical property distributions requires knowledge of the spatial extent of its dolomitisation, in turn requiring understanding of the processes that caused the dolomitisation. Some of this understanding can be derived from measurements but others need to be simulated. In this study the former are used as guides and we focus on the latter, evaluating the character of the dolomitising fluid's movement and temperature patterns by using basin modelling to develop heat-flux simulations to represent the time of dolomitisation. Basin modelling reconstructs the region's geology at the time of dolomitisation while heat-flux simulations recreate the appropriate conductive and convective heat and mass transport through these systems. Potential key drivers are rock mass and fault zone permeability and the position and shape of any salt domes. The results suggest that salt dome shape and position is the dominant control, the salt dome localising convective systems which also use convenient faults so that hotter upwelling fluids pass through the Hasdrubal reservoir and are instrumental in development of burial dolomitisation.

Keywords: Heat-flux simulations burial dolomitisation, basin modelling

INTRODUCTION

Carbonate reservoirs host over 50% of the world's remaining conventional hydrocarbon reserves (Burchette 2012; Garland et al. 2012), but characterising carbonate rock properties where data are sparse remains challenging. The main reason is the well-known tendency of carbonate rocks to undergo extensive, and variably developed, diagenesis that can readily result in one or more order-of-magnitude changes in permeability. Faults and fractures are regarded as potentially important because of their potential to generate significantly heterogeneous permeability fields. Dolomitisation, of interest in this study, and dedolomitisation are also widely recognised for their capability to radically and pervasively change the previous permeability of the affected carbonate rocks. Indeed, 80% of North American and many Middle and Far Eastern carbonate reservoirs are found in dolomitised rocks where dolomitisation is considered to be a major control on reservoir quality (Braithwaite et al. 2004).

In the general case, the main controls on diagenesis are the mineralogy and particle size of sediment, the subsequent thermal and chemical evolution of the pore fluids and, less directly but equally importantly, the structural evolution and the sedimentation rate within the basin (e.g. Machel 2005; Ali et al. 2010). Where the diagenesis takes the form of dolomitisation, of whatever origin, it is generally accepted that it occurs when the pore-fluid chemistry shifts to a magnesium-rich system, causing Ca^{2+} in the carbonate sediments to be replaced by Mg^{2+}.

Dolomitisation can retain, enhance or decrease porosity and permeability (Sun 1995; Lucia 2004; Machel 2004). Although it has been widely studied, important questions regarding the main controls remain (e.g. Hardie 1987; Machel 2004). Generally, occurrence of dolomitisation is limited by slow reaction kinetics (Machel and Mountjoy, 1986) and considered to be most prominent where the temperature is at least 50 to 60°C. With a normal geothermal gradient this temperature is reached at about 1.5 to 2 km. When temperature is less than 50^{o}C, typically above 2km burial depth, the rate of dolomitisation can be very slow because of the slower reaction kinetics. Below 2km, where temperatures are high enough to allow more rapid reaction kinetics, permeability is often so low that the absence of efficient fluid-flow limits the amount of reactive fluids that circulate through the sediments and hence also results in very slow dolomitisation (Machel, 2004). The hydrogeology of the sedimentary basin fill also influences dolomitisation. Sufficient quantities of magnesium-rich pore fluids need to circulate through the rocks, at the right temperature, for dolomitisation to occur at any significant rate (Morrow 1982a, b; Kaufman 1994; Machel 2004; Whitaker et al. 2004). Of equal importance, the larger basin- or sub-basin scale hydrogeological system affects the movement of heat via mobile fluids, particularly via convecting fluid systems.

Reactive transport modelling has been used to explore the spatial distribution of diagenesis (e.g. Chen et al. 1990; Lee 1997; Jones et al. 2000, 2003; Whitaker & Xiao, 2010), in order to establish links between heat-flux, chemical reactions and dolomitisation. Study topics range from hydrothermal dolostones that formed in the vicinity of faults (Corbella et al. 2014) to reactive transport modelling of reflux dolomitisation, early burial dolomitisation and geothermal circulation (Jones et al. 2000, 2003; Whitaker & Xiao, 2010; Garcia-Fresca et al. 2012). However, these studies were largely of a more generic nature, investigating heat-flux and chemical reactions in idealised reservoir geometries to analyse their impact on dolomitisation. Furthermore, even for a modern carbonate system where more subsurface information is available compared to ancient carbonate systems hosting hydrocarbon reservoirs, reactive transport modelling remains challenging because of the scarcity of subsurface data for validation (Whitaker & Xiao, 2010). In addition, applying reactive transport modelling to quantify the extent and magnitude of dolomitisation in carbonate reservoirs remains difficult because the geometry of the reservoir and the sediments' porosity and permeability values prior to dolomitisation, the fluid compositions and temperatures are all difficult to establish (Kaufman 1994; Whitaker et al. 2004).

The work reported here investigates the spatial extent of burial dolomitisation in an Eocene offshore carbonate reservoir, the Hasdrubal Field (e.g. Macaulay et al. 2001; Beavington-Penney et al. 2008; Mangione 2016), using a simulation-centred approach, rather than identifying evidence of mineralogical or geochemical evolution, though all these data are used to help constrain the problem and to support or identify the need for modification of the simulation results. This approach allows us to (1) reconstruct the probable basin geometry and reservoir permeability ranges immediately prior to the dolomitisation and (2) represent these geometries in numerical simulations that aim to provide insights into how basin-scale heat-flux could have impacted reservoir porosity and, more particularly, permeability distributions via permitting dolomitisation to develop in the reservoir. The temperature distributions produced by the simulations are qualitatively compared to the temperatures proposed from assessment of the $\delta^{18}O$ and the fluid inclusion data from the Hasdrubal Field dolomite, which both serve as proxies for temperature; the data indicate that temperature at which dolomitisation occurred was likely in the range of ~78 to 97 °C. This comparison enables us to delineate which heat-flux patterns are consistent with observations and are hence more likely.

The remainder of the paper is structured as follows. In the next section, the geological setting of the study area is discussed, together with the available data, reservoir characterisation and porosity and permeability distribution from subsurface data, and the available oxygen isotope and fluid inclusion data for the dolomite. Then the methods used for the basin modelling and the heat-flux modelling are explained. Finally, the results are presented and analysed.

GEOLOGICAL SETTING

The Hasdrubal Field is in the central area of the Gulf of Gabes on the SE edge of the Pelagian Platform, offshore Tunisia (Figure. 1). Structural events from the Late Permian onwards have influenced the current tectonic setting and the sedimentary fill of the

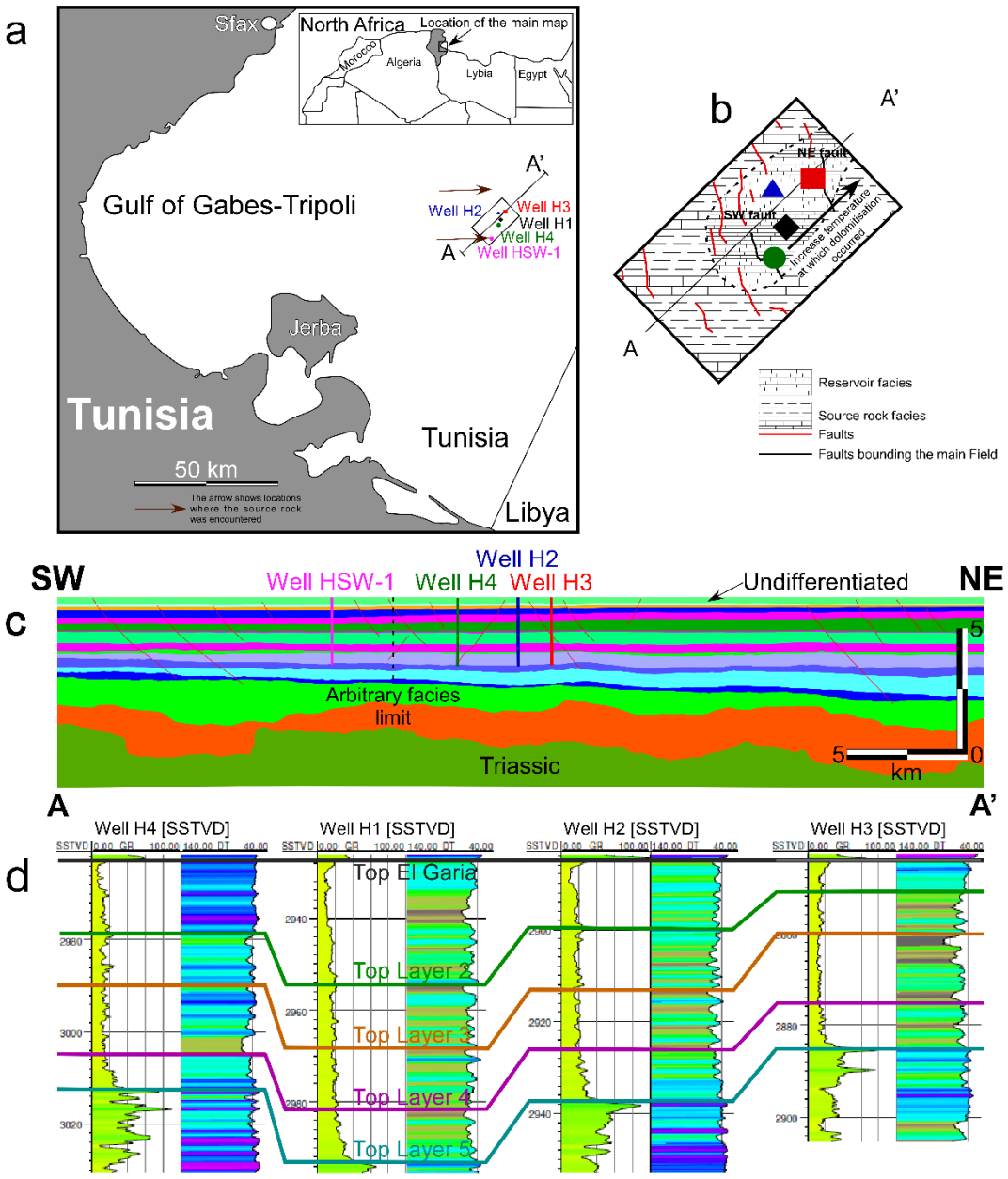

Figure 1. Location and main geological character of the offshore Hasdrubal Field. (**a**) Schematic map showing the location of the Hasdrubal Field. Black rectangle shows location of inset map shown in (b) and line A-A' shows line of schematic cross section shown in (c). Arrows show where source rock was encountered suggesting that the Hasdrubal Field is surrounded by the source rock. (**b**) Inset shows distribution of facies with dashed line showing approximate boundary of the depositional change from reservoir rock to source rock. Faults at top reservoir level shown as red lines, with the SW and NE bounding faults shown in black. Line A-A' is location of cross section. Wells are shown by symbols: red is Well H3; blue is Well H2; black is Well H1 and green is Well H4. (**c**) Cross section A-A' where interval colours are as used in figure 2. Vertical wells have been projected into

the plane of the cross section. (**d**) Gamma ray (left trace) and density-neutron (right trace) logs plotted against true vertical depth for each of the 4 vertical wells. Interpreted Top El Garia Formations and the tops of layers 2, 3 and 4 are labelled and correlated, as shown by lines that connect them (modified from Wynn and Milne, 2010).

Gabes Basin. The main structural elements tend to be oriented NW to SE (e.g. Klett 2001; Racey et al. 2001). Salt was mobilised in the Gulf of Gabes Basin, with diapiric breaching of the Mesozoic and Cenozoic sediments and rocks, and influenced deposition (Bishop 1975; Zaïer et al. 1998; Mejri et al. 2006, Beavington-Penney et al., 2008). During the Early Eocene, the Gulf of Gabes was part of the Southern Tethyan margin, on the southern margin of the Tethys Ocean at a latitude of approximately 21-23° N (Beavington-Penney et al. 2005, 2008). Structural elements such as emergent areas, faults and salt movement, have all influenced deposition of the reservoir interval (e.g. Loucks et al. 1998; Racey et al. 2001; Beavington-Penney et al. 2008).

The Hasdrubal Field is within a NNW-SSE trending horst block approximately 5km by 3.5km in extent (Figure. 1). The main reservoir interval is the Early Eocene (Ypresian) nummulitic, partly dolomitised limestones of the El Garia Formation and is sourced by its lateral equivalent, the Bou Dabbous Formation which is a deep-water organic rich mudstone with planktonic foraminifera (globigerinid), deposited in a deep-water embayment (Macaulay et al. 2001; Racey et al. 2001; Beavington-Penney et al. 2008) (Figure. 2).

During the basinal depositional events that include the El Garia Formation deposition, salt diapirism and fault movements generated structural palaeohighs. However in the Hasdrubal Field, the most obvious effects of salt mobilisation are seen only on the NE margin (Beavington-Penney et al. 2008). This complex palaeobathymetric structural assembly affected the location of the source of the *Nummulites* (Beavington-Penney, 2004), a major component of the El Garia Formation. The Hasdrubal Field's reservoir rocks were primarily allochthonous, mud-rich, nummulithoclastic sediments which also contain abundant in-situ B-form *Nummulites*, (Beavington-Penney et al. 2005; 2008). Some A-form *Nummulites*-dominated grainstones occur locally, typically situated over the presumably less deep active salt domes or fault blocks, and represent deposition in shallow marine, euphotic settings. The Hasdrubal Field is isolated within the facies trend by deep water embayments and it is surrounded by time-equivalent deposits of the Bou Dabbous Formation (Beavington-Penney et al. 2008). This distribution may be related to the complex palaeobathymetry which resulted from a combination of both faulting and salt diapirism.

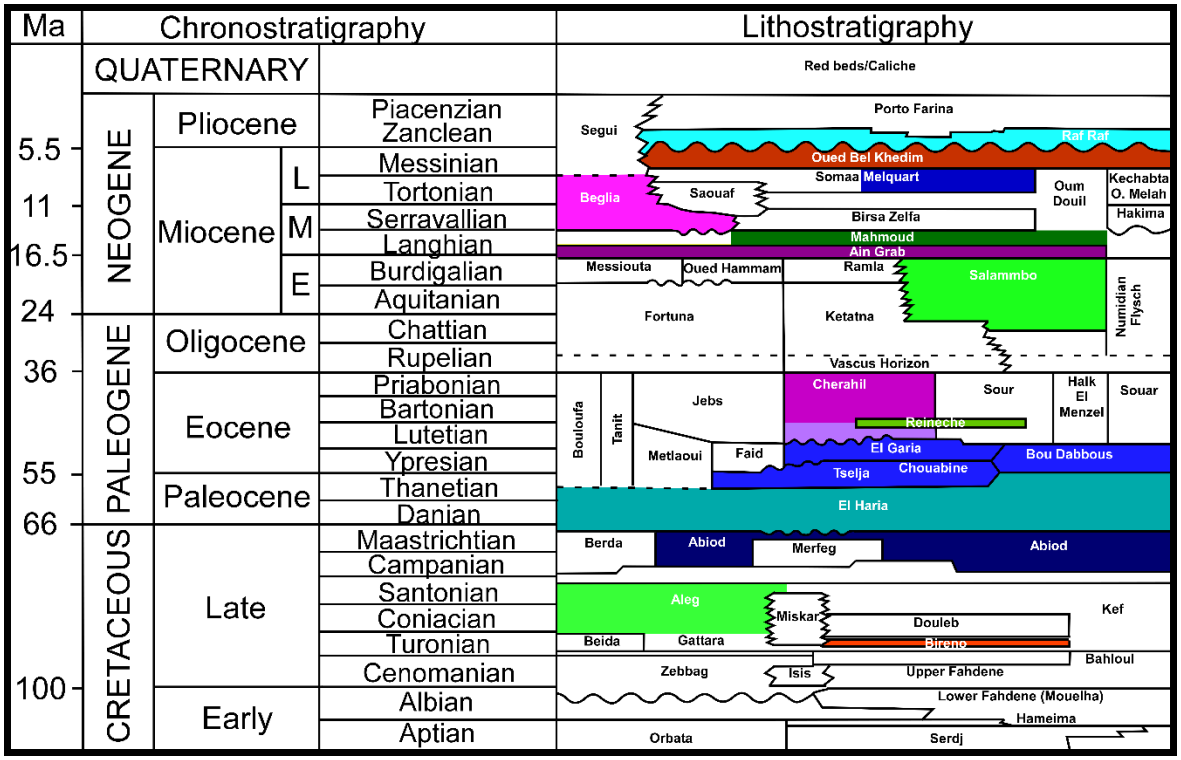

Figure 2. Chronostratigraphy and lithostratigraphy of the study area. Modified from Klett 2001.

Hasdrubal Field and Available Data

The Hasdrubal Field itself is a gas-condensate reservoir with a thin oil rim (Racey et al. 2001) (Figure. 1; Figure. 2) The El Garia Formation, the reservoir interval, is now at almost 3km depth and varies from 40 to 60m thick, thinning and eventually pinching out basinwards where it is replaced by the Bou Dabbous Formation.

The main data made available for this study are a 3D seismic cube, core and core photographs plus a suite of thin sections, proprietary reports and composite logs for the 5 vertical wells (Hasdrubal-1 (H1), -2 (H2), -3 (H3), -4 (H4), and -SW-1 (HSW-1). The fluid pressure, bottom-hole temperature (BHT) and the sparse vitrinite reflectance (VR) dataset for the four vertical wells (Wells H1, H2, H3, H4) were all used in the basin modelling to constrain the fluid pressure conditions and evolution together with the burial and thermal evolution of the reservoir (e.g. Burnham & Sweeney, 1989).

Reservoir characterisation and petrophysical properties

The evolving petrophysical properties of the Hasdrubal Field's carbonate rocks are the result of compaction, both mechanical and chemical, and other diagenetic processes, particularly dolomitisation which is fabric-specific and replaces micrite

(Figure) (Macaulay et al. 2001; Beavington-Penney et al. 2008). Macaulay et al. (2001) divided the reservoir into four layers using a combination of petrophysical properties, variations in grain size and degree of dolomitisation. Their model separates the reservoir into two generally non-dolomitised layers, Layers 1 and 4, at the top and the base of the reservoir respectively and into two more dolomitised layers, Layers 2 and 3. Layer 2 is dominated by A-form *Nummulites* grainstones while Layer 3 consists mainly of packstones and wackestones. In Layers 2 and 3 the matrix is dolomitised to a variable degree (Figure).

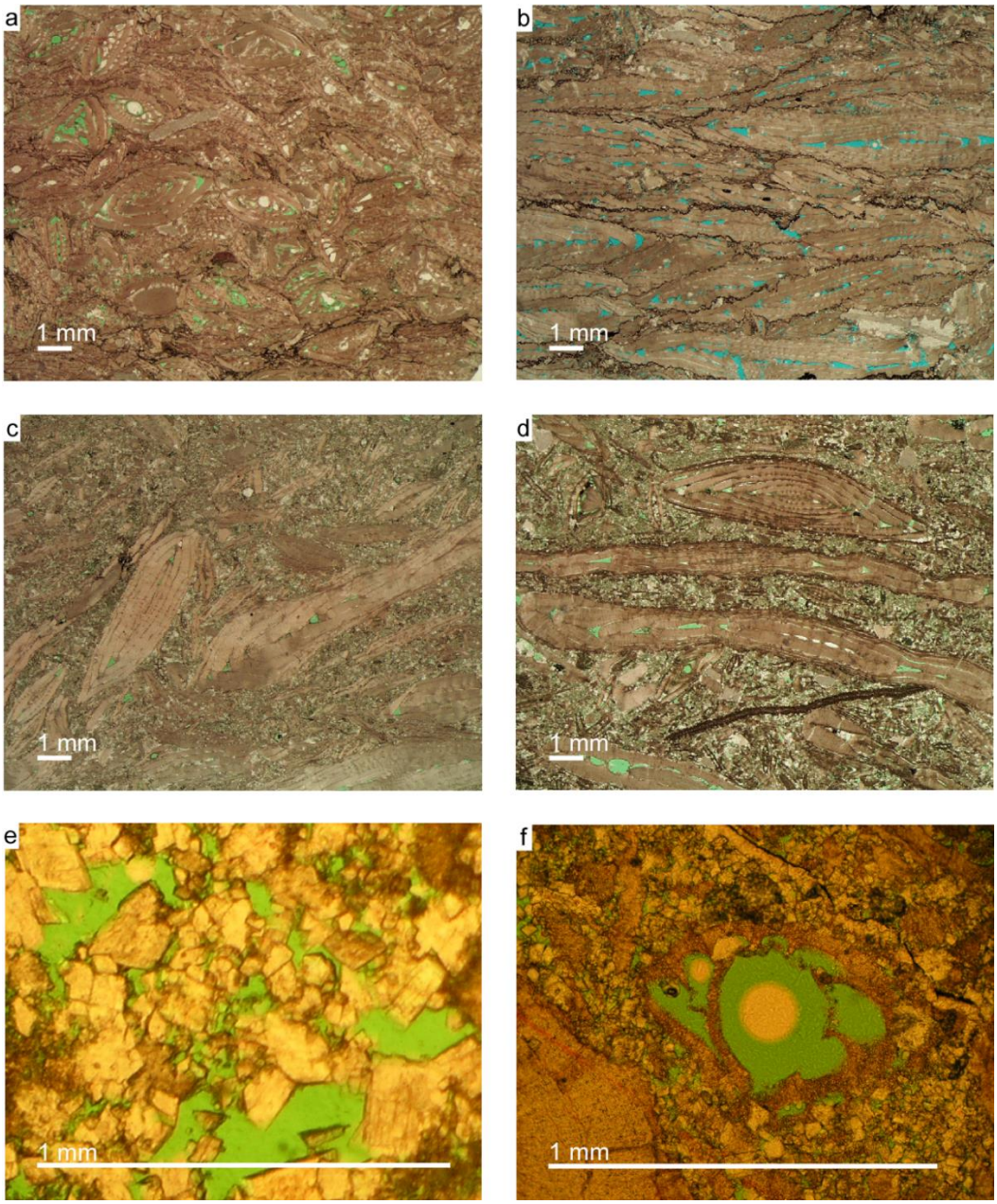

Figure 3. Photomicrographs from Hasdrubal core in the reservoir interval showing intra-particle porosity within *Nummulites* tests and chemical compaction features (a), (b); (c) and (d) show dolomitised micrite; (e) shows inter-crystalline porosity between dolomite crystals and (f) shows dissolved *Nummulites* (e) , (f). See each image for scale bar. The thin sections were stained and the photomicrographs were taken using plane polarized light.

Porosity and permeability data from routine core analysis for wells H2, H3 and H4 show that the highest porosity and permeability are within the dolomitised layers (Figure 4). Porosity varies between ~5 and ~25% in dolomitised layers and between <5 and ~15% in non-dolomitised layers. Permeability generally ranges from ~0.10 to ~30 mD and from less than 0.10 to less than ~10 mD in dolomitised and non-dolomitised layers respectively (Figure 4).

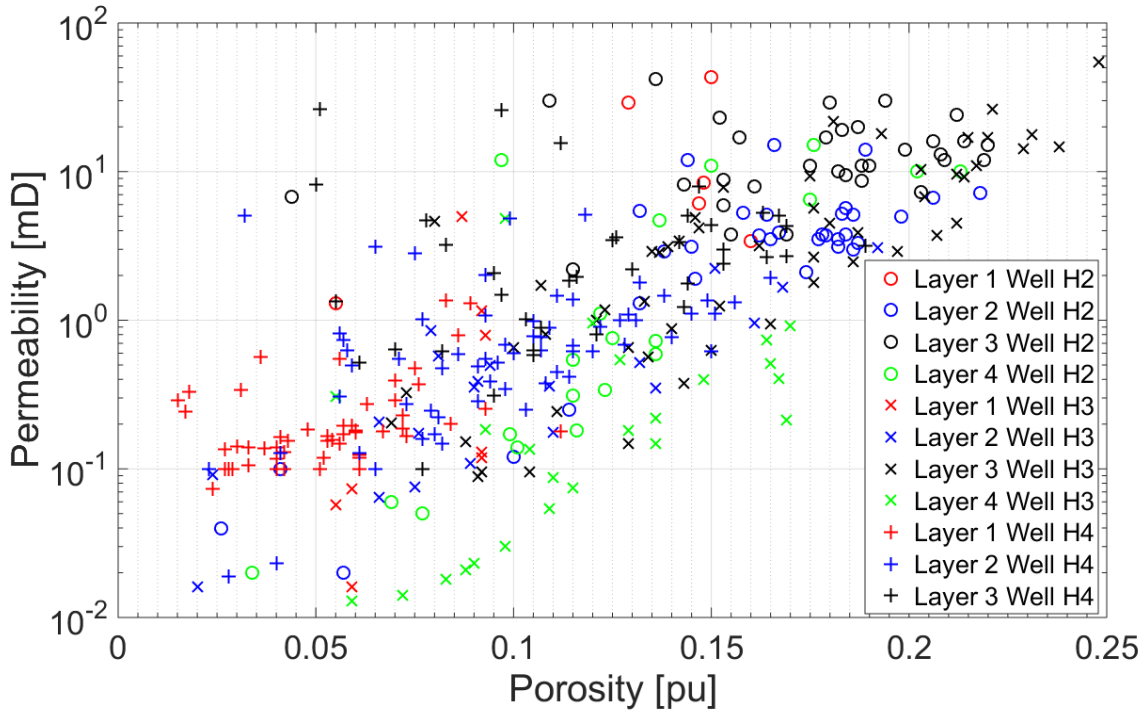

Figure 4. Porosity and permeability of each layer of the Hasdrubal field reservoir rock from routine core analysis. Layers 2 and 3, the dolomitised layers, generally have the highest permeability and Layer 3 in Well H3 has the best reservoir quality.

Typically values of porosity and permeability increase from Well H4 through Well H2 to Well H3 (Figures.1, 2 and 3). The more distal deposits of Well H3 had a higher percentage of micrite prior to dolomitisation than did the shallower, less muddy facies of Well H4, with Well H2 in an intermediate position (Beavington-Penney, 2011). Hence in Well H3 the reservoir rocks can be expected to show a more significant increase in porosity and permeability due to dolomitisation than in the other wells because of the more abundant pre-dolomitisation mud. Within this general trend, Layer 3 in Well H3 has the highest values of porosity and permeability caused also by the development of biomouldic porosity generated after dissolution of *Nummulites* tests (Beavington-Penney, 2011).

Dolomitisation of micrite, enhancing petrophysical properties, has clearly occurred during burial. In fact according to Macaulay et al. (2001) fluid inclusions in dolomite indicate temperatures between ~78 and 89°C for the replaced micrite, and between ~88 and 97°C for the dolomite cement. Macaulay et al. (2001) did use basin modelling to calculate temperature-depth relationships through time but used 1D

modelling to achieve this and so were not able to represent the kinds of lateral variations and consequences for flow patterns being investigated here.

This study replaces the more commonly used starting assumption that the estimated geothermal gradient is approximately uniform with a different approach, as is explained in more detail below. Here the early stage integration of the fluid inclusion data with the burial and thermal history provides a temperature proxy that allows a better estimate of when, and at what depth, dolomitisation occurred in the reservoir. Then a heat-flux simulation is created that represents possible geological and petrophysical conditions at the start of dolomitisation so that the heat-flux patterns that result can be assessed for their ability to produce dolomitisation-friendly temperatures in the reservoir. This issue will be addressed later in the paper where the simulated burial and thermal history is used to provide a more tailored estimate.

Oxygen isotope data and fluid inclusions in dolomite

The oxygen isotope and fluid inclusion data (Table 1; Figure 5) reported by Macaulay et al. (2001) cannot provide sufficient temperature information to identify the dolomitisation process, and so cannot, by itself, adequately constrain the extent of dolomitisation in the reservoir. It is sufficient though to provide a good first order approximation of the thermal regime in the reservoir. Using the generalisation that the more negative the $\delta^{18}O$ values, the hotter the fluid from which dolomite was formed (e.g. Hoefs, 2009), the oxygen isotope and fluid inclusion data were used to rank the different heat-flux simulation results, and so to also rank the geological scenarios on which the simulations were based. As discussed above, the $\delta^{18}O$ value was not converted directly into temperature values in this study, primarily because Macaulay et al. (2001) did not specify in which part of the crystal $\delta^{18}O$ were measured and, depending on where in the crystal the $\delta^{18}O$ were measured, the isotopic signature can vary. Furthermore when, as here, the composition of parent fluids is not completely known this has a strong effect on the calculations (Friedman & O'Neill, 1977; Matthews & Katz, 1977; Vasconcelos et al. 2005). Despite these uncertainties in the $\delta^{18}O$ values of the dolomitised micrite, which acts as a proxy for temperature data at the time of dolomitisation, $\delta^{18}O$ values show a clear trend where the temperature in the vicinity of Well H3 is highest, is intermediate for Well H2 and is lowest in Well H4 (Beavington-Penney 2011).

Note that there is no significant difference between the present-day subsea depth of top of the reservoir at Wells H4 at 2963m TVDSS and H3 at 2845m TVDSS. A structural restoration to the time of dolomitisation shows that the reservoir top was also

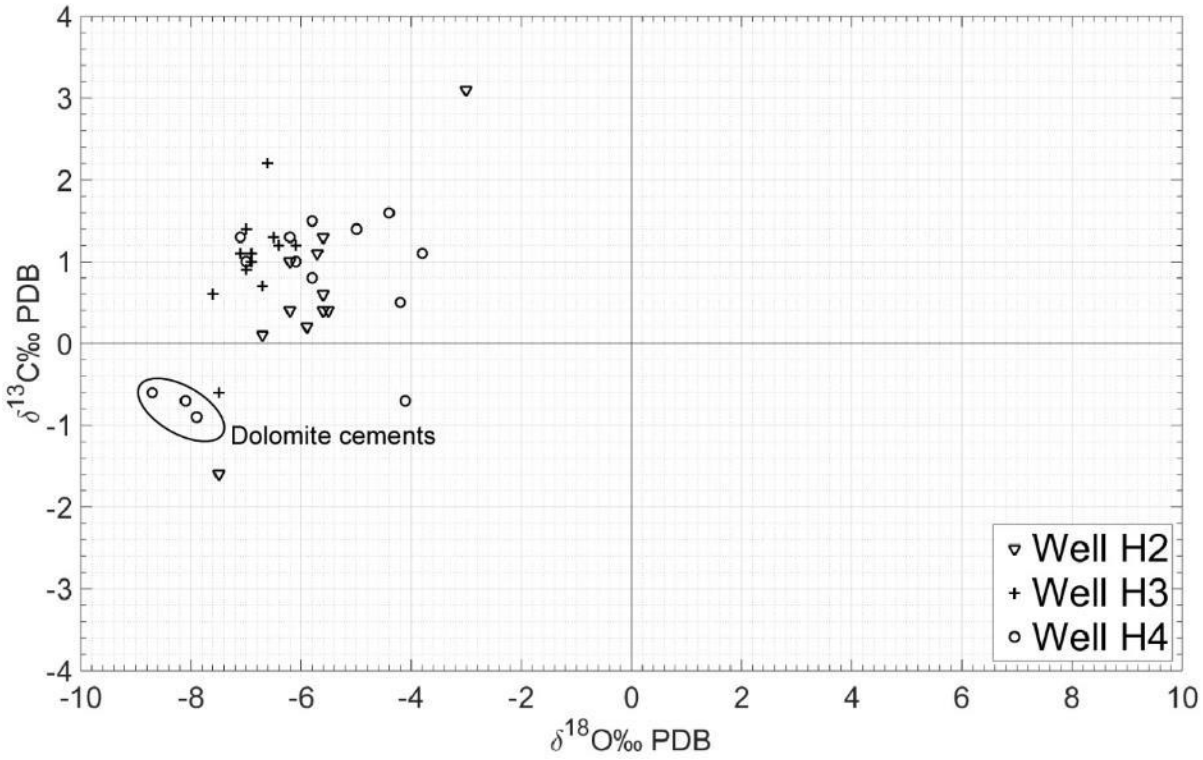

Figure 5. Plot of $\delta^{18}O‰$ PDB (Pee Dee Belemnite) and $\delta^{13}C‰$ PDB of dolomite for wells H2, H3 and H4. Data are taken from Macaulay et al. 2001. $\delta^{13}C‰$ PDB values suggest a marine source of carbon. Samples from well H3 have the lowest values of $\delta^{18}O‰$ PDB whereas samples from Well H4 have the highest values. This distribution of $\delta^{18}O$ suggests that dolomitisation has occurred at highest temperature in the vicinity of Well H3 and lowest in the vicinity of Well H4 (Beavington-Penney 2011).

deeper in Well H4 than in Well H3 (Figure. 6). If a uniform geothermal gradient is assumed across the Hasdrubal Field, it is difficult to explain why the deeper parts of the reservoir, as seen in Well H4, should have experienced lower temperatures than the shallower parts, as seen in Well H3. The hypothesis of this study is that the rate of temperature change with depth is neither uniform nor simply varying but instead is influenced by basin-scale hydrogeological systems which have altered the geothermal gradients from values that would otherwise be expected. In this paper different geological scenarios are investigated in order to analyse the key hydrogeological controls on fluid-flux and hence on heat-flux distribution, and whether basin-scale hydrogeological systems can explain the observed temperature trends.

METHODOLOGY

The method used here has two main parts, basin modelling and heat-flux simulations that are brought together in the later stages of the study. The 1D basin modelling part needs to first establish the time and depth at which the dolomitisation took place before a more detailed 2D basin model is constructed to calculate geometry, burial depth and petrophysical properties throughout the basin, or chosen sub-section of the basin evolution.

Well	Depth [m^2]	Dolomite T [°C]	Salinity [wt% NaCl]	$\delta^{18}O$ data [‰PDB]
H3	2887.0	Matrix 78.1	9.9	-7.5
H3	2887.0	Matrix 88.9	10.1	
H3	2887.0	Matrix 85.2		
H3	2887.0	Matrix 83.3	10.0	
H3	2887.0	Matrix 81.8		
H4	3005.75	Matrix 87.7	10.1	-6.2
H4	3005.75	Matrix 80.9		
H4	3005.75	Cement 88.1	10.6	
H4	3005.75	Cement 92.2	13.7	
H4	3005.75	Cement 94.0	14.2	
H4	3017.0	Matrix 85.3	10.5	-7.1
H4	3017.0	Matrix 82.5	9.7	
H4	3017.0	Cement 96.8	12.8	

Table 1. Fluid inclusions micro-thermometry and salinity data in dolomite samples. Oxygen isotope measurements were also carried out on the same samples (from Macaulay et al. 2001). Note that the published data does not provide measurement errors.

However basin modelling as used here is a non-linear process where the results of the basin model are required in order to create it. This is dealt with in the normal way by using a series of approximations. The first step, or first approximation, is to model the burial and thermal evolution using a 1D simulation at one or more well locations so that each 1D simulation is constrained by the appropriate well data. The simulation results through time are then compared to the temperatures approximated from fluid inclusion data for past geological events to further constrain when dolomitisation occurred at the different well locations. Fluid inclusion micro-thermometry data on a specific diagenetic phase indicate at what temperature that diagenetic phase occurred in the appropriate geological unit. When the burial and

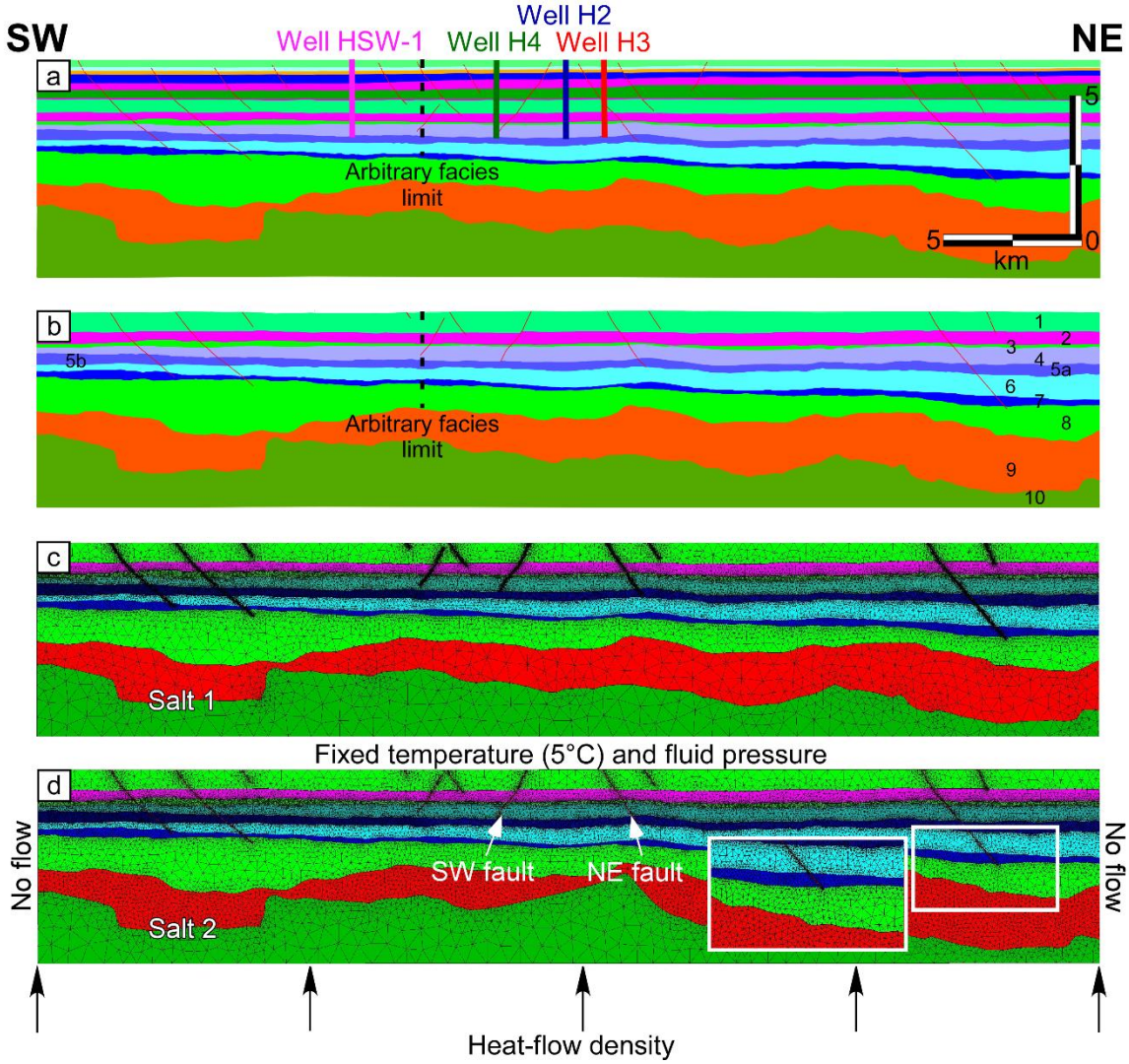

Figure 6. Series of cross sections showing development of the two model geometries that were used for the heat-flow simulations. All cross sections represent the same part of the basin, as shown in Figure. 1a and 1b, and differ in the time period represented and in the interpretation of the shape of the top of the salt. (a) Cross section in the present using Salt 1. Hasdrubal Field wells have been projected into the cross-section. Faults are shown as grey lines and colours for the different rock units are as given in Figure. 1c. Vertical dashed line shows the boundary between reservoir and source rock (b) Cross-section in (a) above has been restored to 32Ma, the interpreted time of dolomitisation. Numbers 1 to 10 represent the different rock units, each with its unique petrophysical properties obtained from basin modelling. Vertical dashed line as in (a). (c) The same cross section as in (b) above using Salt 1. The figure also shows the finite element grid that was used to discretise the model. (d) Cross-section showing Salt 2. This figure also shows the specified boundary conditions and highlights the two faults which bound the reservoir, labelled SW fault and NE fault. Insets show how the geological details of both layers and faults, are preserved; right hand white box identifies area that has been magnified in left hand white box.

thermal history of the same geological unit is known, it is possible to derive the third variable, the timing of the diagenetic event (Dutton & Land 1988; Macaulay et al. 2001).This concept is used to constrain when, and at what depth, dolomitisation occurred in the reservoir. It should be also noted that a slightly bigger range is used

in this study than the range suggested by fluid inclusion data to take into account uncertainties in the data themselves. In spite of some oxygen isotope data being available, it was not used to constrain when, and at what depth, dolomitisation occurred in the reservoir because the conversion from the oxygen isotope value into temperature is affected by too many uncertainties in the Hasdrubal Field. For example an estimate of the parent fluid composition and in which part of the crystal the oxygen isotope value was taken from is needed, but this information was not publically available.

The 1D basin modelling step was followed by a precursor step needed for generating a 2D basin model, a seismic study. The seismic data cube in and around the Hasdrubal Field was used to help choose and generate the most suitable cross section for the 2D basin model. The stage of the 2D basin model which represents the present-day will match the present-day basin geometry as interpreted from the seismic data cube and the resulting basin model output will provide the geometry, petrophysical properties and thermal states at each calculated stage back to the earliest depositional event simulated. This will of course include the step at the chosen time of dolomitisation. The output from the 2D basin model has then provided the basin geometry and rock properties immediately prior to dolomitisation. However given the potential importance of correct geometry, and particularly correct fault geometry a structural restoration using the 2D module of the Move^{TM} suite was used.

The resulting geometry, in 2D, along with the rock properties and the thermal constraints immediately prior to dolomitisation were then used to build a series of high-resolution heat-flux simulations. These simulations replicated the spatio-temporal development of the basin-scale hydrogeological system and the heat-flux pattern that developed within it immediately prior to dolomitisation. The different simulations were similar in most respects, covering variations in parameters identified as potentially significant, namely petrophysical properties of the rock sequence and the fault rocks, as well as the position and shape of the salt domes. The heat-flux simulation results were again compared against the temperature values approximated from oxygen isotope data in order to identify which hydrogeological scenarios were more and less likely.

The heat-flux simulation results were only considered as viable if they provided qualitative agreement between their temperature calculations and the temperatures approximated from oxygen isotope data, i.e. if the eastward increasing temperatures within the reservoir emerged in the simulations.

Basin Modelling

The 1D modelling exercise using the software PetroMod™ were preliminary simulations that allowed us to approximate the thermal and burial history at the different well locations, as outlined above, recognising that the 1D simulations are an approximation to a non-linear problem. The temperature profiles calculated by a 1D basin model for each time step from earliest deposition to the present-day represent the same rocks for which direct and less direct thermal data are available. Both the present-day and the past temperatures and heat-flux values need to be similar to the direct measured and to the less direct thermal data. In effect the 1D simulation results are assessed against measured VR values and present-day bottom-hole temperature. Any significant deviation are noted and the parameters used in the 1D simulation are examined to see if a different, geologically viable, set can produce a better match to the thermal data.

In addition to issues of non-linearity discussed above, there are other limitations inherent to this 1D approach. These limitations include, but are not limited to, possible localised fluid-fluxes that change the rock's temperature but that might not be captured by limited VR data, or by 1D basin modelling. Furthermore, 1D simulation cannot consider spatial heterogeneity in the horizontal direction, and ignores the possibility that fluids can move laterally. Particularly significant for this study, it therefore fails to account for temperature anomalies arising from convective fluid-flux. However, the 1D simulations are still an important precursor to the 2D simulations as they provide information about the approximate geothermal gradients through geological time in the immediate vicinity of each well, but not in between wells. And, as discussed above, they can be used to estimate the time and depth of the initiation of the burial dolomitisation.

The next conceptual step is to generate a 2D basin model using PetroMod™, to obtain information about the evolution of the basin geometry, temperature distribution and petrophysical properties, particularly for the time immediately before the burial dolomitisation which is used to build the 2D flow simulation for the time immediately before burial dolomitisation. A suitable cross-section was identified from the seismic cube. It was not possible to define the base of the reservoir, which is also the top of the Chouabine Formation, from the seismic cube. Also, it was difficult to identify the division between the Chouabine Formation and the older Tselja Formation in the study area (Figure). However because both formations are limestones, this shortcoming is not an issue for the purpose of this study. Hence the reservoir base was represented by the top of El Haria Formation, the same horizon that corresponds to the base of the Tselja Formation. Salt domes have not been penetrated by any wells in the study area but in the seismic cube they appear to be an important feature in the sedimentary basin. However they are at best poorly resolved in the seismic data and their position and shape is a significant geological

uncertainty. Faults are ubiquitous (Figure. 1; Figure. 6) and part of the Hasdrubal Field is bounded by faults.

Following normal practice, a cross section oriented in the tectonic transport direction was chosen, which is also normal to the trend of most of the faults in the area of interest (Figure.1). This cross-section also intercepts Well H3. Wells H2 and H4 are close (300m and 1600m respectively) to this cross section and can be projected on it with a reasonable degree of confidence. After seismic data were converted from the time-domain to the depth domain, the main interpreted horizons and faults were extracted and used to restore the cross section using the software Move™, which is designed to emphasise geometrically correct structural restoration to a series of earliest structural configurations. Using Move™ each layer first decompacted and then restored by sequentially removing faulting and associated structural changes. The Move™ output was then used as input to PetroMod 2D™. Within PetroMod 2D™, the decompaction algorithm of Sclater & Christie (1980) was used. The Sclater and Christie algorithm decreases porosity with depth as shown in equation (1):

$$\varphi = \varphi_0 \, (e^{-cz}), \qquad (1)$$

where φ is present-day porosity at depth, φ_0 is the porosity at the surface, c is the porosity depth coefficient (i.e. the rate of decay of porosity with depth [Km^{-1}]) and z is depth [m]. Restoration was performed back to the time when burial dolomitisation occurred.

This study needs to examine both the dynamic effects of fluid movement, including the potential development of fluid convection, and the petrophysical properties of fault zones. Both convective heat-flux and fault properties are known to impact basin-scale hydrogeological systems (e.g. Lewis & Couples 1999; Matthäi et al. 2004; Davies & Smith, 2006; Wilson et al. 2007; Crutchley et al. 2010, 2013; Lupi et al. 2010, 2011; Saller & Dickson, 2011). In particular the fault zones, need to be represented as deformed areas with specific porosity and permeability distributions so that and movement of fluids across and along the can be well represented. However the 2D basin modelling software addresses fluid movement across fault zones by applying transmissibility multipliers and basin modelling software packages also typically use structured simulation grids. Such structured grids render it difficult to model the geometrical complexity that geological structures such as fault zones represent. So there is a need for a different approach.

Heat-flux modelling

For the reasons outlined above, the reconstructed basin geometry as represented in cross-section, along with the estimated petrophysical properties, are used to build a series of representations of the portion of the basin that contains the Hasdrubal Field at the time that dolomitisation initiated, and minor deviations from it, using CSMP++.

CSMP++ is a simulator that was specifically designed to simulate flow and and mass transport processes in structurally complex geological settings (Matthäi et al., 2007). While there was the possibility of extruding the flow model into the third dimension to permit 3D fluid movement, particularly convection in the fault zones (e.g. Person et al. 2008), because of the computationally complexity already present in the 2D models, it was decided to restrict all simulations to 2D. The simulation replicates the cross-section at the time that dolomitisation starts, as was calculated by the basin modelling. It extends from the deeper parts of the basin at that time, including the salt to the sediment-water interface and away from the reservoir to the northeast and southwest, being approximately 40km in length and 7km thick. While the focus of the study is the reservoir carbonates in the Hasdrubal Field, the CSMP++ simulation is intended to represent the evolution of the basin-scale hydrothermal systems so it is as important to represent the overburden and underburden to the reservoir and the more distant basin shape as it is to represent the reservoir itself.

Starting from a set of boundary and initial conditions, CSMP++ calculates the transient state and calculations are typically continued until a steady state condition is approached. Typically, a simulation was run for at least 350,000 years. The simulation of the basin's hydrogeological system and resulting heat-flux pattern, is performed by solving the standard single-phase advection-diffusion equation for energy conservation (e.g. Ingebritsen et al. 2010):

$$\frac{\partial[\varphi\,(\rho_l h_l)+(1-\phi)\rho_r h_r]}{\partial \mathrm{t}} - \nabla\cdot\left[\frac{\mathrm{k}\rho_l h_l}{\mu_l}\,(\nabla \mathrm{P} + \rho_l\,\mathrm{g}\,\nabla \mathrm{z})\right] - \nabla\cdot \mathrm{K}\nabla \mathrm{T} - \mathrm{S} = 0, \qquad (2)$$

where ρ is the density, h is the specific enthalpy, k is the permeability, μ is the viscosity, P is the fluid pressure, g is the acceleration due to gravity, K is the thermal conductivity of the rock (note that we neglected the contribution of the thermal conductivity of the fluid phase), T is the temperature, S is a thermal source/sink term (e.g. radioactive decay) and the subscripts l and r refer to liquid and rocks respectively. CSMP++ solves this equation using a combination of unstructured finite element and finite volume techniques (Geiger et al., 2006a, b). Using unstructured grids allows fault zones and layers to be represented more realistically and hence preserves their potential effect on the flow systems within the basin, as represented in cross-sections.

Each cross-section used was discretized in space using approximately 70,000 triangular finite elements to create an unstructured finite element grid. Several different levels of grid refinement were tested to ensure that simulation results are not obviously influenced by the chosen mesh but that the number of triangles was not unnecessarily large. Eq. (2) was discretized in in time using an implicit pressure, explicit transport scheme was (Geiger et al., 2006a, b). The equation of state for pure water was used to model the fluid properties. Note that CSMP++ can also simulate the transport of saline fluids (Geiger et al., 2006a, b; Driesner & Heinrich

2007, Weiss et al., 2014). However, as there was no information about past brine compositions, and because previous simulations of combined single-phase heat and salt transport in sedimentary basins showed that the salinity equilibrates quickly (Lupi et al., 2010), we assumed, for simplicity but without loss of generality, that fluid properties are mostly impacted by temperature gradients. Other simplifying assumptions included that chemical reactions were absent, that permeability and porosity remained constant during each simulation for each chosen sedimentary unit, and that the permeability was isotropic for each sedimentary unit.

Boundary and initial conditions

Boundary conditions at the top of the model were defined for fluid pressure and for temperature, the top model pressure replicating the palaeowater depth (≈60 m) obtained from the basin modelling and from any available biostratigraphic data. The top model temperature was fixed at 5°C, the expected temperature at the seafloor-sediment interface and was again consistent with the basin model. These boundary conditions were kept constant throughout the simulation. The model itself was assumed to be at hydrostatic pressure. A constant heat-flux density, derived from the basin modelling for the time of dolomitisation, was applied uniformly across the base of the model. The left and right boundaries were all specified as no flow boundaries for fluid-flow.

The simulations were run until the spatio-temporal changes in temperature became negligibly small, meaning a steady state had been achieved. The final temperature field from each simulation was then compared to the temperature distribution approximated from the oxygen isotope data, allowing a judgement to be made for a given model scenario, of the probability that the given scenario is geologically viable.

Scenarios and sensitivities

A series of scenarios to be used for CSMP++ simulations, plus the reasons for the variations are outlined here. The scenarios are all very similar. Some keep the same structural shape and change only the petrophysical properties assigned to some units in the model. For example, fault zone permeability was changed but the fault zone shape and position were unchanged. Some scenarios altered the shape of the salt dome within the bounds that the geological data permitted. In some cases both types of changes were made.

The basin modelling calculates the evolution of porosity and permeability from deposition through geological time for each layer. The calculated values of porosity and permeability decrease from the top to the bottom of each layer, reflecting the increasing burial depth and associated compaction (Table 1). The largest porosity and permeability values per layer were used in simulations labelled “high case” and the smallest values in simulations labelled “low case”. Sensitivity analysis then assessed how these different scenarios impacted basin-scale hydrogeology and

heat-flux. This set of variations in layer porosity and permeability values was accompanied by a series of simulations of slightly different geological scenarios, that assessed how, for example, fault zone permeability or the location and extent of a salt dome, impacted the hydrogeological system that developed (Table 2 and Figure 5).

Layer number	**ϕ Low case [%]**	**ϕ High Case [%]**	**K Low Case [m^2]**	**K High Case [m^2]**
1	0.35	0.62	5.5×10^{-15}	7.8×10^{-14}
2	0.25	0.37	3.7×10^{-16}	1.2×10^{-15}
3	0.25	0.31	8.9×10^{-14}	1.2×10^{-13}
4	0.15	0.26	1.2×10^{-17}	1.0×10^{-15}
5a	0.30	0.30	1.0×10^{-13}	1.0×10^{-13}
5b	0.13	0.22	8.3×10^{-17}	1.9×10^{-15}
6	0.06	0.15	1.3×10^{-20}	1.2×10^{-18}
7	0.10	0.19	5.5×10^{-15}	9.9×10^{-14}
8	0.049	0.11	9.8×10^{-22}	4.9×10^{-20}
9	0.04	0.10	8.9×10^{-19}	1.0×10^{-17}
10	0.03	0.04	2.6×10^{-20}	4.1×10^{-20}

Table 1. Table showing the layer number and corresponding petrophysical properties used for heat-flow simulations. The values correspond to the low and high cases obtained from the basin modelling.

It was hypothesised that the two parameters that are most likely to affect the hydrothermal system, and so the temperature distribution, are the fault permeabilities and the position of the salt dome (Figure 6).

The presence of a salt dome in a sedimentary basin is regarded as having the potential to generate thermal anomalies in the regions above, below and along the flanks of the salt dome (O'Brien and Lerche, 1987).

No wells in the area have penetrated the salt and all seismic interpretations of the salt position are uncertain, and so the salt's present-day position also remains uncertain. This uncertainty affected the basin restoration and the basin modelling at the time of dolomitisation, and was ultimately brought forward to the heat-flux simulations. In order to analyse how these geological scenarios impact basin-scale hydrogeology and heat-flux, several modelling scenarios have been considered in CSMP++ (Table 2 and Figure 5).

Scenario name	Layer ϕ and k type	Fault k (m^2) *(mD)*	SW Fault k (m^2) *(mD)*	NE Fault k (m^2) *(mD)*	Reservoir k (m^2) *(mD)*	Salt geometry	Thermal conductivity of Salt ($W\ m^{-1}\ K^{-1}$)
LC1	Low case	2.5×10^{-13}	2.5×10^{-13}	2.5×10^{-13}	1.0×10^{-13}	1	3.25
HC1	High case	2.5×10^{-13}	2.5×10^{-13}	2.5×10^{-13}	1.0×10^{-13}	1	3.25
LC2	Low case	2.5×10^{-13}	2.5×10^{-13}	2.5×10^{-13}	1.0×10^{-13}	2	3.25
HC2	High case	2.5×10^{-13}	2.5×10^{-13}	2.5×10^{-13}	1.0×10^{-13}	2	3.25
HC3	High case	1.0×10^{-25}	1.0×10^{-25}	1.0×10^{-25}	1.0×10^{-13}	2	3.25
HC3A	High case	1.0×10^{-25}	1.0×10^{-25}	1.0×10^{-25}	1.0×10^{-13}	2	5.00
HC4	High case	2.5×10^{-13}	2.5×10^{-13}	2.5×10^{-13}	0.5×10^{-13}	2	3.25
HC5	High case	2.5×10^{-13}	2.5×10^{-13}	2.5×10^{-13}	1.0×10^{-15}	2	3.25
HC6	High case	2.5×10^{-13}	1.5×10^{-13}	2.5×10^{-13}	1.0×10^{-13}	1	3.25
HC7	High case	2.5×10^{-13}	2.5×10^{-13}	1.5×10^{-13}	1.0×10^{-13}	1	3.25
HC8	High case	2.5×10^{-13}	1.5×10^{-13}	2.5×10^{-13}	1.0×10^{-13}	2	3.25
HC9	High case	2.5×10^{-13}	2.5×10^{-13}	1.5×10^{-13}	1.0×10^{-13}	2	3.25

Table 2. Summary of the model scenarios discussed in this study.

The two different geometries of the salt dome are shown in Figure. 6c (Salt1) and Figure. 6d (Salt 2). The seismic data were also not of sufficient resolution to allow precise identification of the relationships between the faults and the four layers into which the reservoir of the Hasdrubal Field is divided. The reservoir is currently contained within a horst block, which was also present in a similar form at the time of dolomitisation. In the heat-flux simulations, the faults that delimitate this horst block are referred to as the SW and NE faults. Assigned fault permeabilities ranged from closed faults (i.e. 1.0×10^{-25} $m^{2,}$ approximately $1.0 \times 10^{-7}\mu D$) to open faults (i.e. $2.5 \times 10^{-13} m^2$ that is approximately 250mD); the permeabilities of faults SW and NE close to the Hasdrubal Field were altered to reflect probable differences in fault

permeability (1.5×10^{-13} m^2 and 2.5×10^{-13} m^2 , or 150 and 250 mD respectively were used) consistent with expected ranges of rock damage generation due to the faulting process (Table 3; Figure 5). For simplicity all other faults retained their previous permeabilities though it is equally likely that they could also have increased or decreased permeabilities due to rock damage during faulting. Well HSW1 penetrated the source rock (Figure. 1), which indicates that the reservoir terminated somewhere between Well HSW1 and its nearest neighbour Well H4, and was replaced by source rock. Lacking any better control, a vertical reservoir boundary was introduced at equal distance between these two wells.

In total, 40 different scenarios were simulated, but for brevity only the results of the 12 most interesting are reported (Table 3). All other scenarios not shown here yield results that do not differ in any meaningful way from any of the results presented below.

RESULTS

Basin modelling

The basin modelling began with the 1D simulations of each well with temperature data that allowed an approximation to the thermal and burial conditions. These results then informed the 2D simulations which are the main part of the basin modelling work. The first step was to use the present-day temperature data to assess the present-day heat-flux values calculated in the 1D basin model (Figure. 7). Once a decent match between simulation-generated and measured temperatures had been obtained, the VR data from the wells and as calculated by the basin model simulation were compared (Figure 8). This approach, while initially seeming a little clumsy, was followed for the following reasons: (1) the available VR data were sparse, being one value each for Wells H2, H3 and H4 and seven for Well H1; (2) the burial and structural history is similar for each well and the wells are close; (3) there was a possibility of capturing some of the inherent spatial variations in heat-flux pattern. Note that three values of VR from Well H1 were excluded because they were unrealistically low for the given depth.

The VR data of Wells H1, H2 and H3 were matched by the 1D basin models when a heat-flux density of 56 mW/m^2 was used for all the wells from the time of reservoir unit deposition to the present. This heat-flux density value is close to the 59 mW/m^2 suggested by McQuilken (1998) for this area. However, a higher heat-flux density of

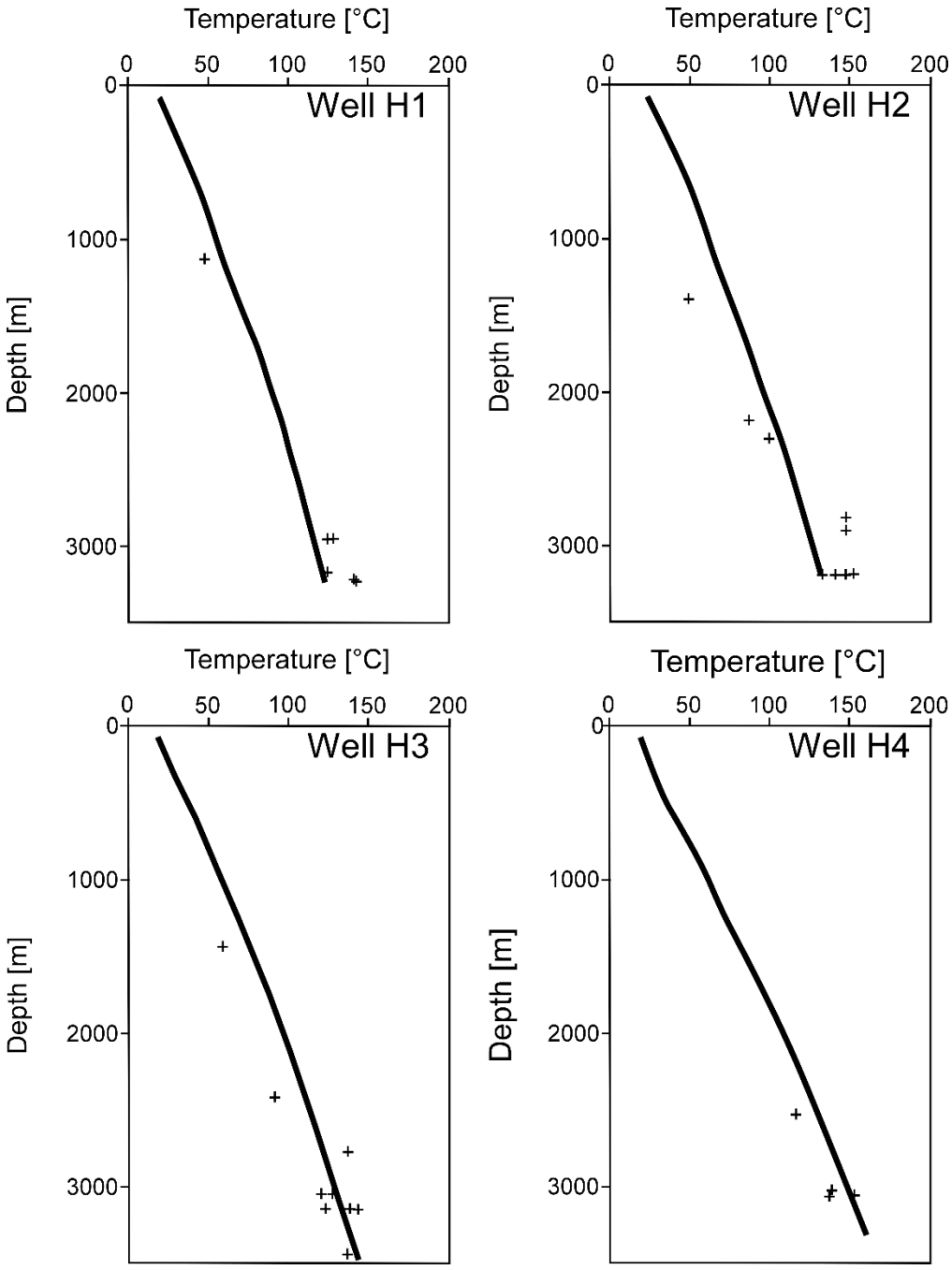

Figure. 7. Present-day temperature profiles at wells H1, H2, H3 and H4. The crosses indicate the measured present-day temperature and the lines are the geothermal gradients estimated from 1D basin modelling.

80 mW/m^2, again from the time of reservoir unit deposition to the present-day was required to match the VR data for Well H4, together with a value of 70 mW/m^2 to match the present-day temperatures at this well. These values are above the heat-flux density of 68 mW/m^2 suggested by McQuilken (1998), but are still reasonable considering the uncertainties surrounding the estimation of past heat-flux densities and thermal conductivities.

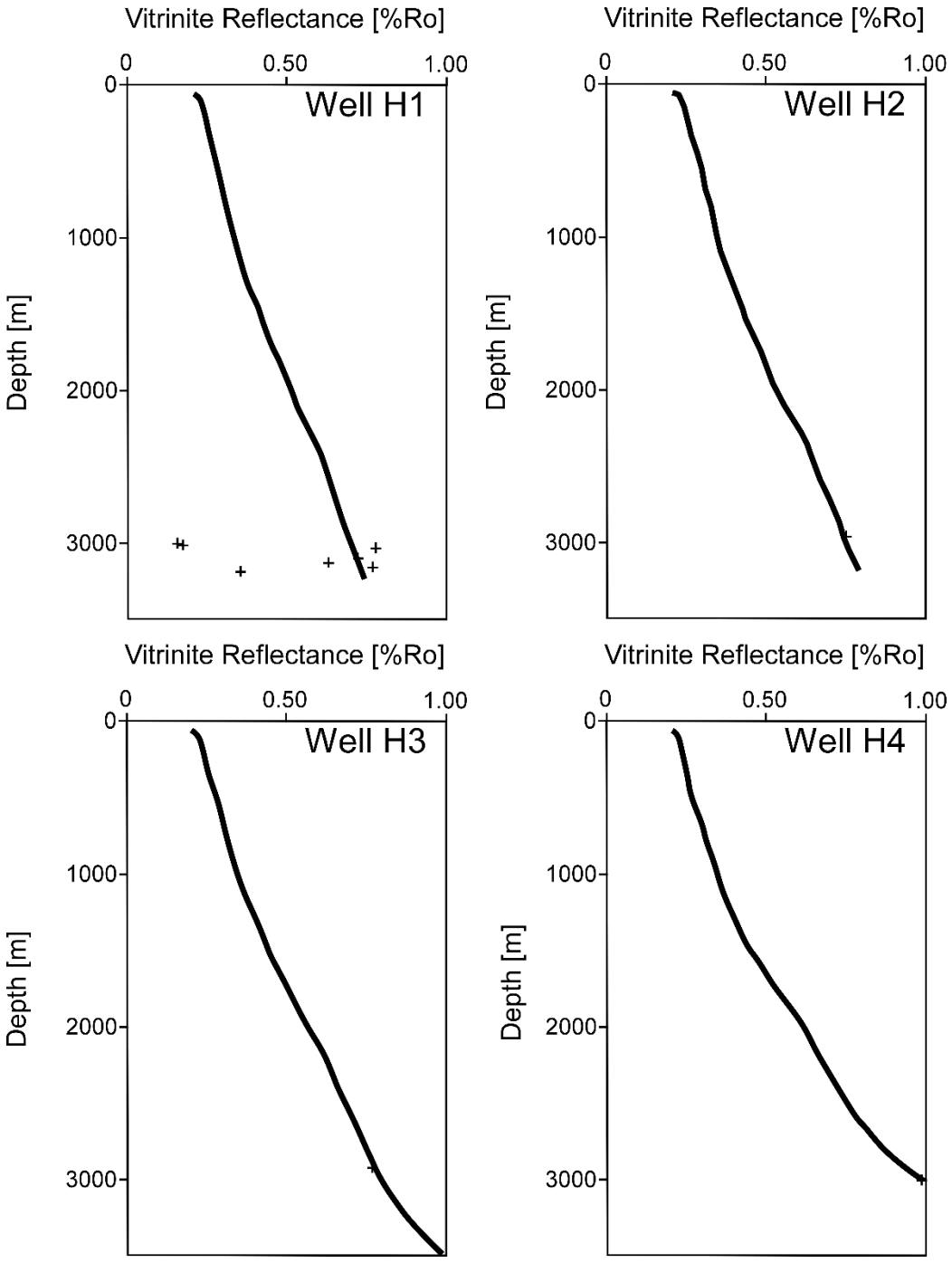

Figure 8. Measured VR and calculated VRe for wells H1, H2, H3 and H4 The VRe is obtained from the 1D basin modelling for each well. The measured data is shown as crosses and the calculated VRe is plotted as a line.

The next step was to use the calibrated 1D models to determine, as best as possible, the time and depth conditions which bracket the temperatures of reservoir dolomitisation. This step includes temperature comparisons and any other suitable geological information. As noted above, the problem is a non-linear one, with both the basin model calculations and the temperatures calculated from the fluid inclusion data containing assumptions that require the solution of this step. However one has to start somewhere. The basin modelling results were compared with the temperatures approximated from the fluid inclusion data (Figure). Macaulay et al.

(2001) suggested that dolomitisation occurred at temperatures between ≈78 and ≈97°C. However as explained above, a slightly larger temperature range from 70 to 100°C was explored to ensure that uncertainties related to the fluid inclusion data themselves were included. Basin modelling results suggested that reservoir temperatures reached the broader dolomitisation temperature range between ≈35 and ≈12 Ma (Figure. 9). Petroleum generation and migration commenced ≈20 Ma (McQuilken 1998; Racey et al. 2001). Since no petroleum inclusions were observed in the dolomite samples (Macaulay et al 2001), dolomitisation had probably occurred before hydrocarbon migration. The fact that dolomitisation improved reservoir quality further lends evidence to the observation that dolomitisation occurred before petroleum migration. Hence dolomitisation probably occurred between ≈35 and ≈20 Ma, which agrees with the hypothesis of Macaulay et al. (2001) that dolomite formation coincides with the onset of rapid burial and heating in the early Miocene (≈23 Ma).

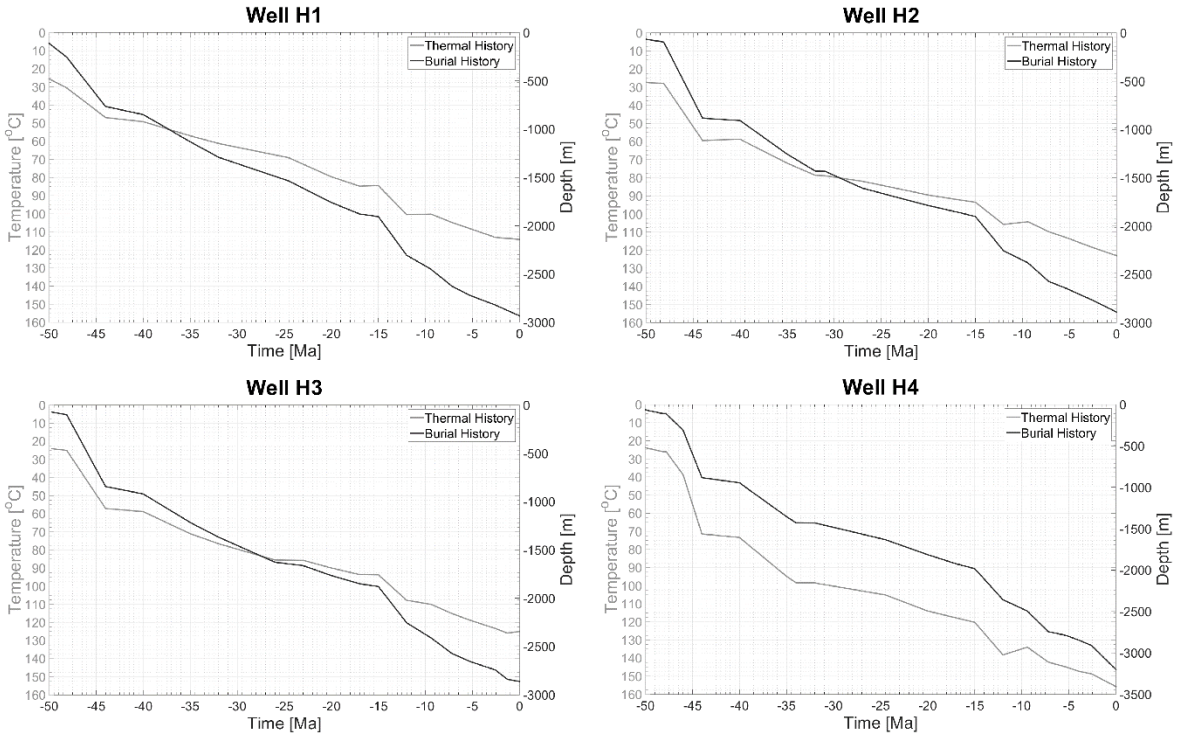

Figure 9. Results from 1D basin modelling showing temperature and burial history of the top of the reservoir at each of the four wells H1, H2, H3 and H4. Time is shown on the x axis and both calculated temperature and burial depth are shown on the y axis.

Based on these results, the geometry of the basin at 32Ma derived from the structural restoration analysis, as discussed above, and the thermal, physical and petrophysical properties of the layers from the basin modelling, were used to construct the 2D basin model and is shown in Figure. 6. Note that the other end member scenario, the basin geometry at 20 Ma, is indistinguishable from the basin geometry at 32 Ma except for the deposition of the Ain Grab Formation. Since the Ain Grab Formation is presently only approximately 50m thick, its possible impact on basin scale hydrogeology was already covered by the range of permeability

scenarios considered in the heat-flux simulations. Hence only the basin geometry at 32 Ma was used in the heat-flux modelling.

Heat-flux simulations

As discussed above, the 1D basin modelling calculations suggested that basal heat-flux density values could have vary between 59 mW/m^2 (Well H1) to 70 or even 80 mW/m^2 (Well H4). A sensitivity analysis over this range of showed that the basal heat-flux density does not change the spatio-temporal evolution of the temperature field though it does change the value of the maximum temperature. Hence, only results using 70 mW/m^2 as the basal heat-flux density are shown here. See Table 3 for the name of the model scenarios used in this section.

Scenarios LC1 and HC1 (Table 3) are both assigned the same petrophysical properties for the reservoir (1.0×10^{-13} m^2 or approximately 100 mD), the same isotropic fault zone permeability of 2.5×10^{-13} m^2, or approximately 250mD, and the same salt shape (Salt 1). But they differ in the petrophysical properties of the non-reservoir units, with LC1 using the low- and HC1 the high-end cases. In scenario LC1 there is hardly any variation in the temperature profile between the start and end of the simulation (here after 100,000 years). In contrast, scenario HC1 shows clear convection in the basin. The final temperature distributions for each case, together with the difference in temperature from the initial to the final step are shown in Figure . This figure also shows the calculated temperature profiles at wells H2, H3, and H4 at the end of the simulation. Figure 10b shows only a few degree difference in temperature in a few locations near faults developed during scenario LC1. This is consistent with little to no convection having developed in this scenario, very probably due to the low permeability of the non-reservoir unit. In contrast, scenario HC1, which develops temperature changes up to 30°C hotter and colder than the starting temperature around several fault zones shows clear evidence of convection.

As discussed above, the dolomitisation temperature at Well H3 was probably higher than at Well H4 and dolomitisation occurred at intermediate temperatures at Well H2. However, Figure e and Figure f show that the calculated temperature gradients along a vertical lines at each of the well locations do not replicate this pattern, which suggests that both scenarios are probably a poor match to the geology represented by the model.

Scenarios LC2 and HC2 (Table 3; Figure 1) are considered next. They have the same petrophysical properties as do scenarios LC1 and HC1 but both use a different salt shape (Salt 2). As before, scenario LC2 is dominated by conduction and the simulated temperature gradients at the location of the three wells are all very similar. However scenario HC2 is dominated by convection as shown by deviations in the isotherms where temperatures both 30°C higher and lower than the background around fault zones.

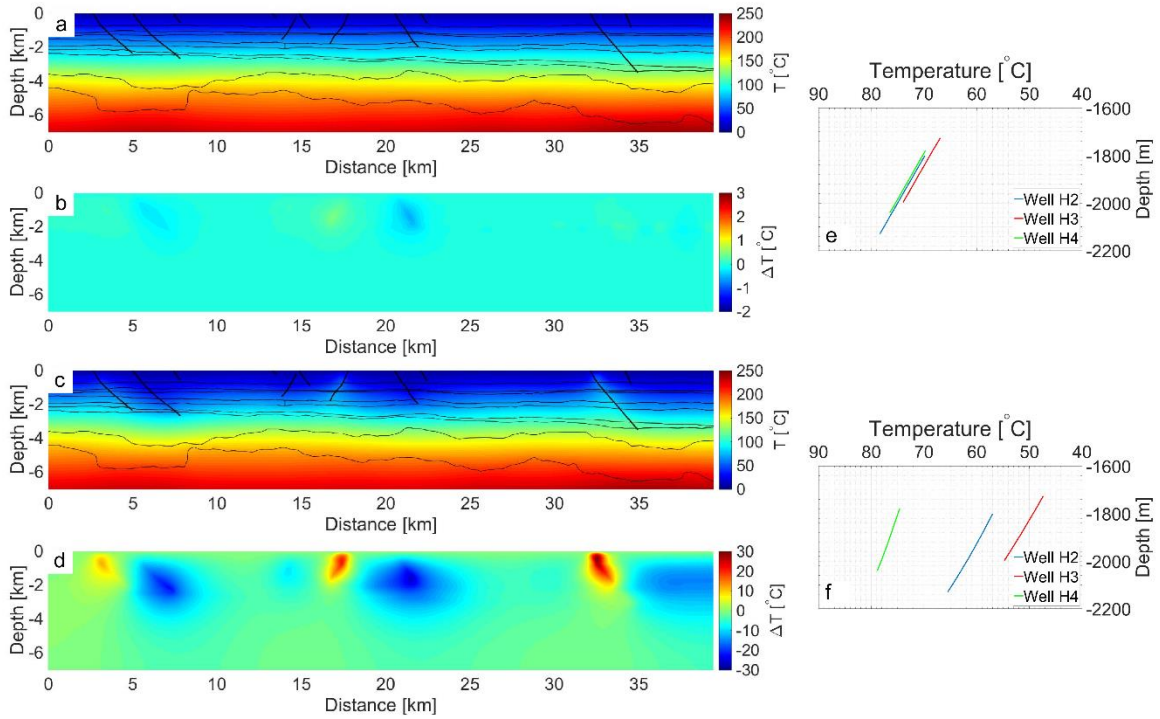

Figure 10. Temperature and temperature difference results of the simulations LC1 and HC1. See Table 3 for the different scenarios. (**a**) Shows for scenario LC1 the temperature at the end of the simulation. (**b**) Shows for scenario LC1 the difference between the start (conduction only) and end (convection and conduction) of the simulation. (**c**) Shows for scenario HC1 the temperature at the end of the simulation. (**d**) Shows for scenario HC1 the difference between the start (conduction only) and end (convection and conduction) of the simulation. Note the marked difference in temperature at the end of the simulation. (**e**) and (**f**) show the geothermal gradients obtained from the simulation at the position of the wells H2, H3 and H4 for scenarios LC1 and HC1, respectively.

In scenario HC2, temperature gradients at the wells are consistent with the temperatures patterns obtained from the oxygen isotope data: reservoir rocks in Well H3 have the highest temperature, Well H2 has intermediate temperatures, and Well H4 reservoir rocks are the coldest. This indicates that the position of the salt influences the convection pattern, that scenario Salt 2 produces a better match to the basin hydrogeology, and that convection was probably present in the basin, influencing the fluid temperatures and so the pattern and locations of reservoir dolomitisation. This does not necessarily mean that scenario Salt 2 is the correct salt interpretation, but just that the change in salt configuration, combined with somewhat permeable fault zones, can permit convection in some cases and preclude it in others. Because of the interest in the thermal effects of convection of reservoir dolomitisation, no further low end cases are shown.

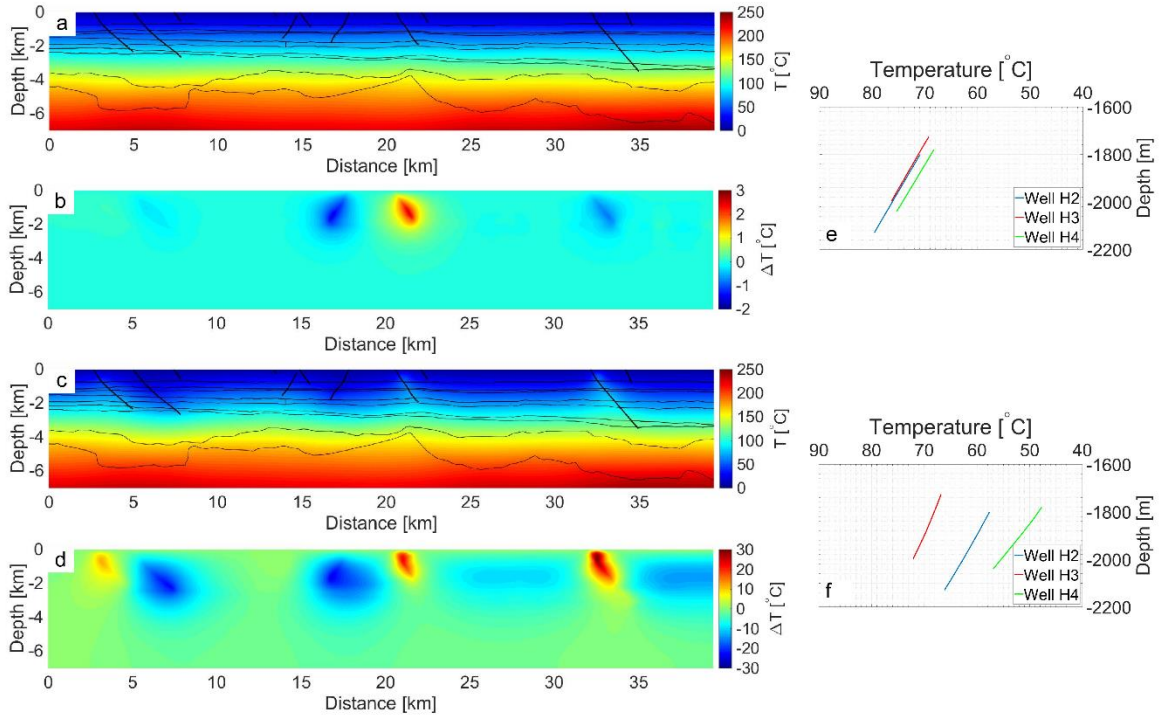

Figure 1. Temperature and temperature difference results of the simulations LC2 and HC2. See Table 3 for the different scenarios. (**a**) Shows for scenario LC2 the temperature at the end of the simulation. (**b**) Shows for scenario LC2 the difference between the start (conduction only) and end (convection and conduction) of the simulation. (**c**) Shows for scenario HC2 the temperature at the end of the simulation. (**d**) Shows for scenario HC2 the difference between the start (conduction only) and end (convection and conduction) of the simulation. Note the marked difference in temperature at the end of the simulation. (**e**) and (**f**) show the geothermal gradients obtained from the simulation at the position of the wells H2, H3 and H4 for scenarios LC2 and HC2, respectively.

Scenarios HC3 and HC3a are identical to HC2 in most respects. The significant difference is a reduction of the fault zone permeability by 12 orders of magnitude, from 2.5 x 10^{-13} m^2 (approximately 250mD) in HC3 to 1 x 10^{-25} m^2 (approximately 1.0 x 10^{-4} μD) in HC4, making the faults impermeable. These two scenarios differ in the chosen salt thermal conductivity, with HC3 using 3.25 $Wm^{-1}K^{-1}$, the value used in all previous scenarios, representing a mixture of salt and other lithologies present in the stratigraphic column and HC3A uses 5.0 W $m^{-1}K^{-1}$ representing almost pure salt (Figure 2). The extremely low fault zone permeabilities result in calculated temperature changes of only one or two degrees (Figure. 12b and d) strongly suggesting only conductive heat movement. Unsurprisingly the calculated well temperature profiles vary only slightly from each other (Figure. 12e and f) and are not consistent with the observed well temperature. These scenarios confirm that the fault zone needs to be permeable enough for convection to develop.

Scenarios HC4 and HC5 both use Salt 2, with the petrophysical properties of the non-reservoir units being the high case. The fault zone permeabilities are the same as were used in all scenarios except HC3 and HC3A.

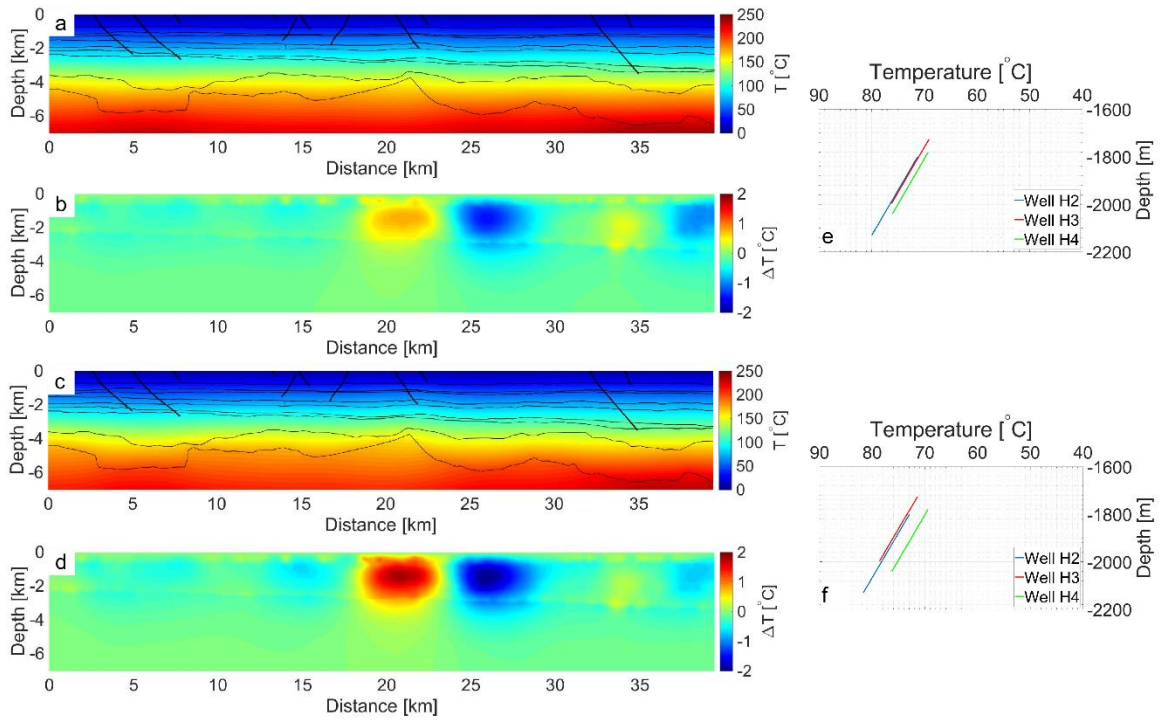

Figure 2. Temperature and temperature difference results of the simulations HC3 and HC3a. See Table 3 for the different scenarios. (**a**) Shows for scenario HC3 the temperature at the end of the simulation. (**b**) Shows for scenario HC3 the difference between the start (conduction only) and end (convection and conduction) of the simulation. (**c**) Shows for scenario HC3a the temperature at the end of the simulation. (**d**) Shows for scenario HC3a the difference between the start (conduction only) and end (convection and conduction) of the simulation. (**e**) and (**f**) show the geothermal gradients obtained from the simulation at the position of the wells H2, H3 and H4 for scenarios HC3 and HC3a, respectively.

But scenario HC4 uses a reservoir permeability that is half that of all previous scenarios while HC5's reservoir permeability is two orders of magnitude smaller than all previous scenarios, approximately 1mD. As is apparent in Figure 3, scenario HC4 shows that, in spite of the reservoir interval being slightly less permeable, convection patterns emerge that are consistent with the temperature trends observed in the wells. In contrast, and unsurprisingly, scenario HC5 shows that a reservoir permeability of 1mD suppresses convection and the temperature differences between individual wells are too small. This supports the expectation that very low reservoir permeabilities were unlikely at the time of dolomitisation but equally that reservoir dolomitisation does not require very high reservoir permeabilities.

Scenarios HC6, HC7, HC8 and HC9 attempt to assess the relative contributions to development of convection, and particularly to development of convection within the Hasdrubal Field, of fault zone permeability and the salt shape. In pair HC6 and HC7, the SW and NE fault zones, which bound the Hasdrubal Field, are assigned different permeabilities, such that in HC6, the SW fault has 1.5 x 10^{-13} m^2 (approximately 150mD) permeability and the NE fault 2.5 x 10^{-13} m^2 (approximately 250mD) permeability (Table 2).

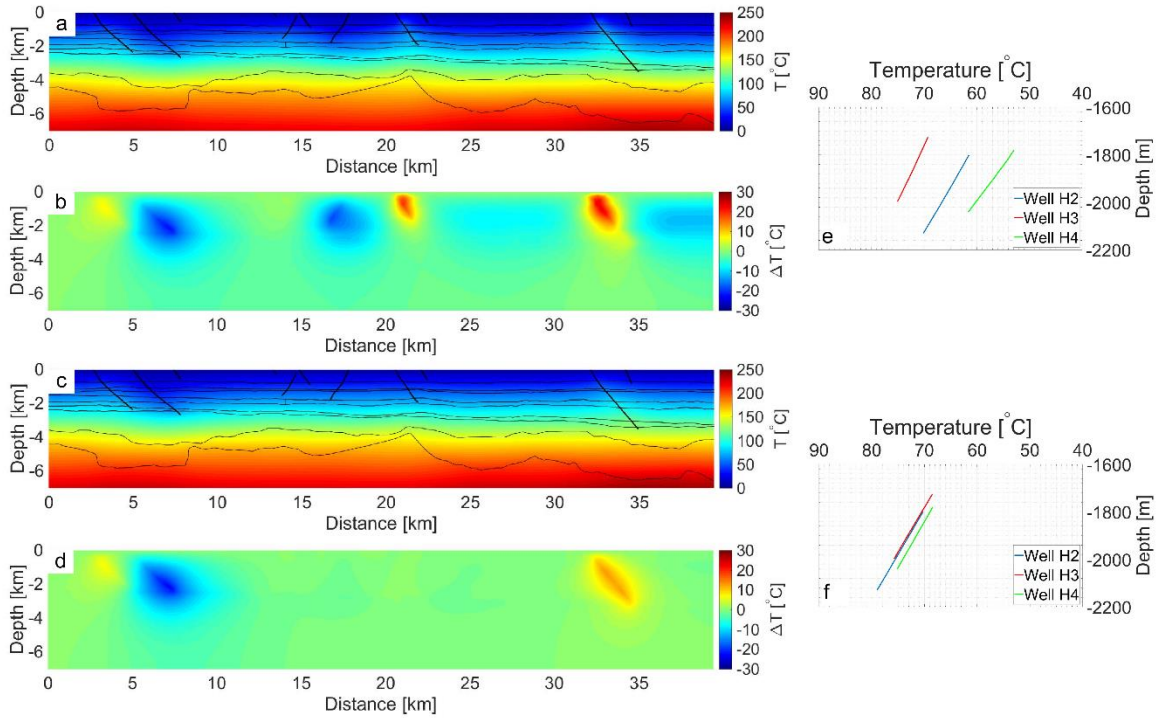

Figure 3. Temperature and temperature difference results of the simulations HC4 and HC5. See Table 3 for the different scenarios. (**a**) Shows for scenario HC4 the temperature at the end of the simulation. (**b**) Shows for scenario HC4 the difference between the start (conduction only) and end (convection and conduction) of the simulation. (**c**) Shows for scenario HC5 the temperature at the end of the simulation. (**d**) Shows for scenario HC5 the difference between the start (conduction only) and end (convection and conduction) of the simulation. (**e**) and (**f**) show the geothermal gradients obtained from the simulation at the position of the wells H2, H3 and H4 for scenarios HC4 and HC5, respectively.

These are inverted in scenario HC7. Salt 1 is used for both scenarios. Pair HC8 and HC9 vary from HC6 and HC7 only in their use of Salt 2.

Figure 14 shows that scenarios HC6 and HC7 both develop convection but the resulting temperature profile does not agree with the temperature trends at the wells. Scenarios HC6 and HC7 are very similar to HC3, varying only in the permeability of faults.

However scenarios HC8 and HC9 (Fig 15) shows that, irrespective of the fault permeability range used here use of Salt 2 results in convection patterns, and calculated temperature profiles at the wells, that agree qualitatively with the temperature trends observed for the wells. There are, of course, some quantitative differences, for example the simulated geothermal gradient in the vicinity of Well H4 is steeper in scenarios HC8 than HC9. This set of results supports the contention that fault zone permeability is a factor, but it is the different positions of the salt dome that has the stronger influence on the basin-scale hydrogeology.

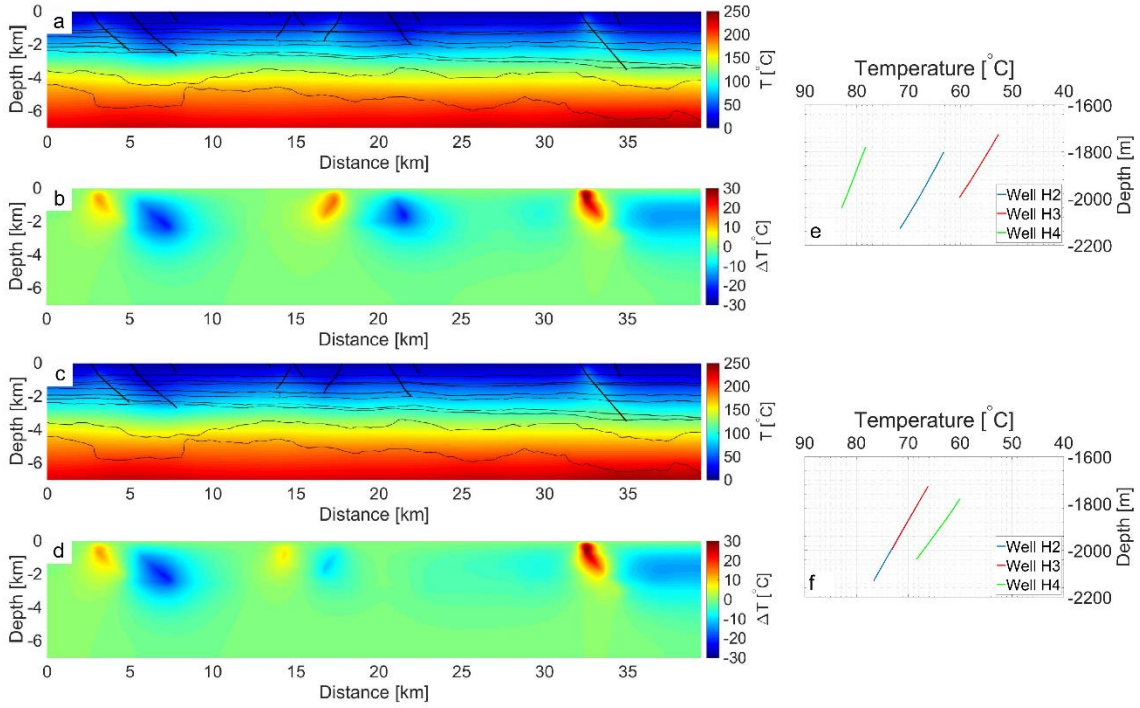

Figure 14. Temperature and temperature difference results of the simulations HC6 and HC7. See Table 3 for the different scenarios. (**a**) Shows for scenario HC6 the temperature at the end of the simulation. (**b**) Shows for scenario HC6 the difference between the start (conduction only) and end (convection and conduction) of the simulation. (**c**) Shows for scenario HC7 the temperature at the end of the simulation. (**d**) Shows for scenario HC7 the difference between the start (conduction only) and end (convection and conduction) of the simulation. (**e**) and (**f**) show the geothermal gradients obtained from the simulation at the position of the wells H2, H3 and H4 for scenarios HC6 and HC7, respectively.

This observation holds true for the scenarios tested but it is recognised that a robust conclusion would require a wider set of fault permeability scenarios. Never the less this work indicates that the shape of the salt layer is an important factor. As discussed previously, the aim of this study was to identify any qualitative agreement and consistency and not to obtain a quantitative match between temperatures derived from oxygen isotope data and numerical simulations.

The result that fault zones contribute to basin-scale heat-flux, but that their impact is less than the top shape and position of the salt layers is unexpected, particularly considering that high-permeability faults are often observed or modelled to be the main flow conduits for buoyancy-dominated fluid flow in basins (e.g. Lewis and Couples , 1999; Bächler et al., 2003; Harcouët-Menco et al., 2009; Lupi et al., 2010; Kampman et al., 2012; Person et al., 2012; Guillou-Frottier et al., 2013). There are several potential reasons for this. One is that the fault permeabilities used in this study are lower than those used by the authors listed above, in which case one value of this study is to put a lower bound on the dominance of salt shape over fault zone permeability. Another is that heat-flux in the third dimension is an important factor in

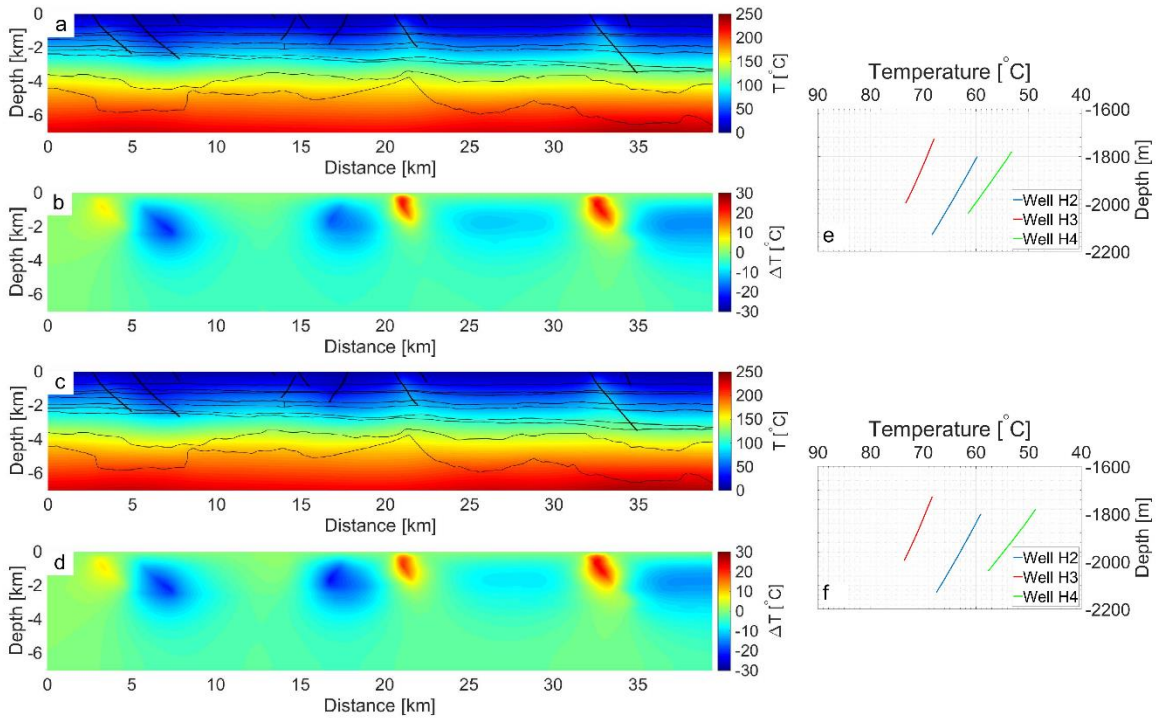

Figure 15. Temperature and temperature difference results of the simulations HC8 and HC9. See Table 3 for the different scenarios. (**a**) Shows for scenario HC8 the temperature at the end of the simulation. (**b**) Shows for scenario HC8 the difference between the start (conduction only) and end (convection and conduction) of the simulation. (**c**) Shows for scenario HC9 the temperature at the end of the simulation. (**d**) Shows for scenario HC9 the difference between the start (conduction only) and end (convection and conduction) of the simulation. (**e**) and (**f**) show the geothermal gradients obtained from the simulation at the position of the wells H2, H3 and H4 for scenarios HC8 and HC9, respectively.

many situations, within the fault zones or within the basin as a whole. A third reason could be the variation of fault permeability with time such that, for example, faults in seismically active basins can act as valves that release excess pore pressure and reach much higher permeabilities than those considered here, albeit for only very brief periods (e.g. Stanislavsky and Garven, 2003; Sibson 2007; Lupi et al. 2011). Another reason could be the difficulties in imaging faults close to salt so that the seismic interpretations and consequent models are missing some faults which, if included, could lead to more convection. However, since there are no data that supports short-lived increases in fault permeability, or faults that extend below the salt layers in this study area, these hypotheses have not been tested.

DISCUSSION

The primary aim of this study was to assess, using heat-flux simulations, a series of scenarios for their ability to produce the basin-scale convective flow systems needed for burial dolomitisation in the Hasdrubal reservoir. The simulations show that convective systems did develop in a subset of simulations and that some of these simulations also produced temperatures consistent with such information from the wells in the Hasdrubal Field.

The method required simulations of the basin at the time of dolomitisation, between ≈35 and ≈20 Ma. Basin modelling, which is extremely well suited to calculating prior burial depths, thicknesses and partially decompacted petrophysical properties was used. In this case because the structural evolution also mattered, structural restoration was also used to refine the structural shapes. However basin modelling is not designed to perform precise fluid- or heat-flux simulations. In particular there is no way to simulate convection. So the heat-flux simulations are essential to reveal the basin-scale hydrogeological system.

However, as well as the expected limitations resulting from incomplete basin and reservoir data, there are inevitably limitations to this modelling method which uses a combination of basin modelling, structural restoration and heat-flux simulations.

The analysis begins with 1D basin models at the location of the vertical wells in the Hasdrubal Field. While the results of this initial step are not particularly sensitive to small differences in VR data, three of the four wells have only one VR data point and more robust 1D basin models can be generated with more reliable VR data. The present-day geological cross-section, which forms the basis of the 2D basin modelling exercise relies heavily on interpretation of seismic data. However, as is normally the case, these data were not sufficient to allow a confident identification of all horizons. In particular the top and base of the salt are difficult to determine with a high degree of certainty and this resulted in the need to use two quite different salt geometries. While the geometry called Salt 2 provided a better match to the subsurface temperature and heat information available, there is no independent information to suggest that Salt 2 is a good match to the actual top and base of the salt.

There are also always uncertainties associated with the decompaction of the basin fill during the 2D basin modelling. There is no specific reason though for this to be a particular problem in this study as we tested different permeability ranges in the heat-flux simulations. There are issues that arise, however, in using the results of the basin model to populate the heat-flux geomodel. In particular, the basin modelling subdivides each geological unit into a specified number of subunits, and for decompaction calculations, treats each sublayer separately producing a relatively smooth variation in porosity and permeability with depth in that geological unit. However it is not practical to include this degree of detail in the heat-flux simulations, so an upper and lower estimate of porosity and particularly permeability have been included in the study (Tables 2 and 3), though it is recognised that both are approximations. The heat-flux geomodel uses a flexible gridding method and is capable of a very good approximation to the geometry any geological layer, and particularly to the faulting, replicating both fault offset and fault width and permitting the fault rock to be assigned appropriate petrophysical properties.

The heat-flux simulations require boundary conditions of the type described in the Methodology section. While these are relatively flexible they do not permit variations in temperature at the geomodel top or in heat-flux density at the base, restricting the match to reality slightly. The basin fluids were assumed to be pure water instead of basin brine. While fluid inclusion data provided insights into fluid temperature and salinity at the time of dolomitisation, the available data were not sufficient to constrain the salinity of the basin brine and the default of pure water was preferred. But saline brines can alter convection patterns to some degree as compared to pure water fluids (Geiger et al., 2005). It is also likely that the fault permeabilities, as well as the permeabilities of the individual sedimentary layers, are non-uniform. But in the absence of additional data, and considering that the petrophysical data were derived using decompaction curves, the approach chosen was to keep the permeability of the individual layers and faults uniform, rather than introducing improperly constrained heterogeneities and also complicating the model building stage. There are other types of data that could help to constrain the geomodel and make it more robust. Possible data sources include, but are not limited to the following: (i) facies analysis in the seismic, (ii) 3D structural restoration which may be able to constrain the position of any salt, (iii) experimental data, for carbonate rocks such as oedemeter experiments could help building appropriate decompaction curves, which are much needed for carbonate rocks.

The heat-flux simulations were designed to mimic flow systems in 2D at the basin scale but with the faults represented as zones for which different permeabilities can be assigned. This choice inevitably has consequences. The main recognised risk that within-fault convection, as described by Person et al. (2008), is missed, though it is also entirely feasible for convection to develop in the direction normal to the chosen cross-section direction within the sedimentary layering, in much the same way as it has done in the plane of the cross-section. And such currently out-of-plane convection could develop in different locations to those observed in this study. There is also the inevitable simplification of geometries, property distribution and boundary conditions inherent to all simulations. The choice of the series of scenarios was designed to mitigate this risk in this study in much the same fashion as is done in other such studies. The risks identified have been described and discussed above.

CONCLUSIONS

The timing and cause of burial dolomitisation in the Hasdrubal Field, an offshore carbonate reservoir, has been investigated using a combination of 1D and 2D basin modelling and basin-scale heat-flux modelling. Dolomitisation occurred, according to fluid inclusion data, at temperature ranging from ~78 to ~97 °C and has enhanced the reservoir quality of the micrite-rich facies.

Oxygen isotope data suggest that dolomitisation occurred at highest temperatures in the NE part of the basin and decreased towards the SW. We hypothesised that basin-scale hydrogeological processes caused these temperature variations and redistributed Mg in the reservoir. We hence reconstructed the burial-thermal history of the reservoir using 1D basin modelling that was constrained to temperature, pressure and VR data. We obtained the approximate timing of dolomitisation from these 1D simulations and could hence use this information to constrain the 2D basin modelling and structural restoration, which provided us with a representative cross-section of the basin geometry at the time dolomitisation occurred, as well as the relevant petrophysical properties.

We used the petrophysical properties, the restored cross section and the boundary conditions provided by the basin modelling to set-up several high-resolution heat-flux simulations to explore how the basin-scale hydrogeology and resulting heat-flux patterns have impacted temperature distribution at the time of dolomitisation, considering a variety of possible geological model scenarios. Simulation results were compared to temperature trends apparent in the oxygen isotope data to rank different geological models. A key outcome of this analysis was that basin-scale convective fluid-flow, and hence moderately high permeabilities of the sedimentary layers, are required for dolomitisation to occur. A key structural feature that controlled the hydrogeological system that was favourable for dolomitisation in the Hasdrubal Field was the position of a basal salt dome while, somewhat surprisingly, fault permeability did not have a great influence on convection patterns. As a general conclusion from this, basin modelling should not rely only on conductive heat-flux modelling but also consider convective fluid-flow in order to approximate basin-scale heat-flux patterns appropriately.

ACKNOWLEDGEMENTS

We thank BG Group and Petrobras for providing funding for this project through the International Centre for Carbonate Reservoirs (ICCR1), a joint research alliance between Heriot Watt University and the University of Edinburgh. We are in debt to Dr Frances Abbots, Dr Richard Steele, Siham Ghomari, Chokri Chiboub and ETAP (Entreprise Tunisienne d'Activités Pétrolières). We thanks Schlumberger for access to the PetroMod™ software package which was used extensively in this study and Midland Valley for access to their 3D Move software suite as well as free training for A Mangione. We are also very grateful to the ICCR team, both ICCR1 and ICCR2, for many fruitful discussions. S.G thanks Foundation CMG for supporting his chair in carbonate reservoir simulation.

BIBLIOGRAPHY

Ali, S., Clark, W., Moore, W., & Dribus, J., 2010. Diagenesis and reservoir quality. Oilfield Review 22 (2), 14–27.

Bächler, D., Kohl, T., & Rybach, L. 2003. Impact of graben-parallel faults on hydrothermal convection–Rhine Graben case study. Physics and Chemistry of the Earth, Parts A/B/C, 28(9), 431-441.

Beavington-Penney, S., 2004. El Garia Formation Lithofacies Analysis, Gulf of Gabes, Tunisia. BG Group, Internal Report, pp. 1–54.

Beavington-Penney S.J. 2011. An Alternative Model for Controls on Flow in the Hasdrubal Reservoir: Implications for Petrel Property Modelling. BG Group Internal report, 1-9.

Beavington-Penney, S.J., Nadin, P., Wright, V.P., Clarke, E., McQuilken, J., & Bailey, H.W. 2008. Reservoir quality variations on an Eocene carbonate ramp, El Garia Formation, offshore Tunisia: Structural control of burial corrosion and dolomitisation. Sedimentary Geology, 209, 42-57.

Beavington-Penney, S.J., Wright, V.P., & Racey, A., 2005. Sediment production and dispersal on foraminifera-dominated early Tertiary ramps: the Eocene El Garia Formation, Tunisia. Sedimentology 52, 537–569.

Bishop, W. 1975. Geology of Tunisia and adjacent part of Algeria and Lybia. AAPG Bulletin 59 No3, 413-450.

Braithwaite, C.J.R., Rizzi, G., & Darke G. 2004. The geometry and petrogenesis of dolomite hydrocarbon reservoirs: introduction. Geological Society, London, Special Publications, 235, 1-6. doi: 10.1144/GSL.SP.2004.235.01.01

Burchette, T.P. 2012. Carbonate rocks and petroleum reservoirs: a geological perspective from the industry. Geological Society, London, Special Publications, 370(1): 17–37,doi: 10.1144/SP370.14.

Burnham, A.K. & Sweeney, J.J. 1989. A chemical kinetic model of vitrinite maturation and reflectance. Geochimica et Cosmochimica Acta, 53, 2649-2657.

Chen, W., Ghaith, A., Park, A. & Ortoleva, P. 1990. Diagenesis through coupled processes: Modeling approach, self-organization, and implications for exploration. American Association of Petroleum Geologists, Memoir, 49, pp. 103-130.

Corbella, M., Gomez-Rivas, E., Martín-Martín, J.D., Stafford, S.L., Teixell, A., Griera, A.,Travé, A., Cardellach E. & Salas R. 2014. Insights to controls on dolomitization by

means of reactive transport models applied to the Benicàssim case study (Maestrat Basin, eastern Spain). Petroleum Geoscience 20, 2014, 41–54 http://dx.doi.org/10.1144/petgeo2012-095.

Crutchley, G.J., Berndt, C., Geiger, S., Klaeschen, D., Papenberg, C., Klaucke, I., Hornbach, M.J., Bangs, N.L.B. & Maier C., 2013. Drivers of focused and prolonged fluid flow and methane seepage at South Hydrate Ridge, offshore Oregon, USA. Geology, 41(5), 551-554, doi:10.1130/G34057.1.

Crutchley, G.J., Geiger, S., Pecher, I.A., Gorman, A.R., Henrys, S.A. & Zhu H., 2010. The potential influence of shallow gas and gas hydrates on sea floor erosion of Rock Garden, an uplifted ridge offshore of New Zealand. Geo-Marine Letters, 30, 283-303, doi:10.1007/s00367-010-0186-y.

Davies, G.R., & Smith, Jr., L.B. 2006. Structurally controlled hydrothermal dolomite reservoir facies: An overview. AAPG Bullettin, 90, 11, 1641-1690.

Driesner, T., & Heinrich, C. A. 2007. The system H2O–NaCl. Part I: Correlation formulae for phase relations in temperature–pressure–composition space from 0 to 1000° C, 0 to 5000bar, and 0 to 1 X NaCl. Geochimica et Cosmochimica Acta, 71(20), 4880-4901.

Dutton, S. P., & Land, L. S. 1988. Cementation and burial history of a low-permeability quartzarenite, Lower Cretaceous Travis Peak Formation, East Texas. Geological Society of America Bulletin, 100(8), 1271-1282.

Friedman, I. & O'Neill, J.R. 1977. Compilation of stable isotope fractionation factors of geochemical interest. In Fleischer, M. (Ed.) Data of Geochemistry, 6th edn, USGS Professional Paper 440-KK.

Garcia-Fresca, B., Lucia, J.F., Harp Jr., J. & Kerans, C. 2012. Outcrop constrained hydrogeological simulations of brine reflux and early dolomitization of the Permina San Andres Formation. AAPG Bullettin, 96, 1757, 1781.

Garland, J., Neilson, J., Laubach S.E. & Whidden, K.J. 2012. Advances in carbonate exploration and reservoir analysis. Geological Society, London, Special Publications, 370(1):1–15, doi: 10.1144/SP370.15.

Geiger, S., Driesner, T., Heinrich, C. A., & Matthäi, S. K. 2005. On the dynamics of NaCl-H2O fluid convection in the Earth's crust. Journal of Geophysical Research: Solid Earth, 110(B7), 1-23.

Geiger, S., Driesner, T., Heinrich, C.A. & Matthäi, S.K. 2006a. Multiphase thermohaline convection in the Earth's crust: I. A novel finite element-finite volume

solution technique combined with a new equation of state for NaCl-H2O. Transport in Porous Media, 63, 399-434.

Geiger, S., Driesner, T., Heinrich, C.A., & Matthäi, S.K. 2006b. Multiphase thermohaline convection in the Earth's crust: II. Benchmarking and application of a finite element–finite volume solution technique with a NaCl–H2O equation of state. Transport in Porous Media, 63(3), 435-461.

Harcouët-Menou, V., Guillou-Frottier, l., Bonneville, A., Adler, P. M., & Mourzenko, V. 2009. Hydrothermal convection in and around mineralized fault zones: insights from two-and three-dimensional numerical modeling applied to the Ashanti belt, Ghana. Geofluids, 9(2), 116-137.

Guillou-Frottier, L., Carrė, C., Bourgine, B., Bouchot, V., & Genter, A. 2013. Structure of hydrothermal convection in the Upper Rhine Graben as inferred from corrected temperature data and basin-scale numerical models. Journal of Volcanology and Geothermal Research, 256, 29-49.

Hardie, L.A. 1987. Dolomitization: a critical view of some current views. Journal of Sedimentary Petrology, 57, 166-183.

Hoefs, J. 2009. Stable isotope geochemistry, Springer, 1-285.

Ingebritsen, S. E., Geiger, S., Hurwitz, S., & Driesner, T. 2010. Numerical simulation of magmatic hydrothermal systems. Reviews of Geophysics, 48(1), 1-33.

Jones, G.D., Smart, P. L., Whitaker, F. F., Rostrom, J.B. & Machel, H.G. 2003. Numerical modeling of reflux dolomitization in the Grosmont platform complex (Upper Devonian), Western Canada sedimentary basin: AAPG Bulletin, 87, 8, 1273–1298, doi: 10.1306/03260302007.

Jones, G. D., Whitaker, F. F., Smart, P. L. & Sanford W. E. 2000. Numerical modeling of geothermal and reflux circulation in Enewetak Atoll: Implications for dolomitization: Journal of Geochemical Exploration, v. 69–70, p. 71–75, doi: 10.1016/S0375-6742(00)00010-8.

Kampman, N., Burnside, N. M., Shipton, Z. K., Chapman, H. J., Nicholl, J. A., Ellam, R. M., & Bickle, M. J. 2012. Pulses of carbon dioxide emissions from intracrustal faults following climatic warming. Nature Geoscience, 5(5), 352-358.

Kaufman, J. K., 1994. Numerical models of fluid flow in carbonate platforms: Implications for dolomitization: Journal of Sedimentary Research, A64, 128–139.

Klett., T.R. 2001. Total Petroleum Systems of the Pelagian Province, Tunisia, Libya, Italy, and Malta—The Bou Dabbous–Tertiary and Jurassic-Cretaceous Composite. U.S. Geological Survey Bulletin, 2202-D, 1-149.

Lee, M.K. 1997. Predicting diagenetic effects of groundwater flow in sedimentary basins: a modeling approach with examples. In: Montañez, l.E, Gregg, J.M. & Shelton, K.L. Basinwide Fluid Flow and Associated Diagenetic Patterns: Integrated Petrographic, Geochemical, and Hydrologic Consideration. Society of Economic Paleontologist and Mineralogists, Special Publications, 57, pp. 3-14.

Lewis, H., & Couples, G.D. 1999. Carboniferous basin evolution of central Ireland-simulation of structural controls on mineralization. Geological Society, London, Special Publications, 155: 277-302, doi: 10.1144/GSL.SP.1999.155.01.19. In: K.J.W. Mccaffrey, L. Lonergan and J.J Wilkinson (eds) Fractures, Fluid Flow and Mineralization, Geological Society, London, Special Publications, 151, 277 302.

Loucks, R.G., Moody, R.T.J., Bellis, J.K. & A.A. Brown. 1998. Regional depositional setting and pore network systems of the El Garia Formation (Metlaoui Group, Lower Eocene), offshore Tunisia. In: MacGregor, D.S., Moody, R.T.J., Clark-Lowes, D.D. (Eds.), Petroleum Geology of North Africa. Geological Society of London Special Publication,132, 355-374. voi 10.1144/GSL.1998.132.01.20. In: D.S. Macgregor and D.D. Clark-Lowes (eds) 1998. Petroleum Geology of North Africa. Geological Society, London, Special Publication No. 132, 355-374.

Lucia, F. J. 2004. Origin and petrophysics of dolostone pore space. Geological Society, London, Special Publications 2004, Vol. 235, pp. 141-155. doi 10.1144/GSL.SP.2004.235.01.06. From: C.J.R. Braithwaite, G. Rizzi and G. Darke (eds). The Geometry and Petrogenesis of Dolomite Hydrocarbon Reservoirs. Geological Society, London, Special Publications, 235, 141-155.

Lupi, M., Geiger S, & Graham CM. 2010. Hydrothermal fluid flow within a tectonically active rift-ridge transform junction: Tjörnes Fracture Zone, Iceland. Journal of Geophysical Research, 115, B05104, doi: 10.1029/2009JB006640.

Lupi, M., Geiger S. & Graham C.M. 2011. Numerical simulations of seismicity-induced fluid flow in the Tjoernes Fracture Zone, Iceland. Journal of Geophysical Research, 116, B07101, doi: 10.1029/2010JB007732.

Macaulay, C.I., Beckett, D., Braithwaite, K., Bliefnick D. & B. Philps. 2001. Constraints on diagenesis and reservoir quality in the fractured Hasdrubal field, offshore Tunisia. Journal of Petroleum Geology, 24, 55-78.

Machel, H. G. 2004. Concepts and models of dolomitization: a critical reappraisal. Geological Society, London, Special Publications, 2004, 235, 7-63. doi:

10.1144/GSL.SP.2004.235.01.02. From: Braithewaite, C. J. R., Rizzi, G. & Darke, G. (eds) 2004. The Geometry and Petrogenesis of Dolomite Hydrocarbon Reservoirs. Geological Society, London, Special Publications.

Machel, H., 2005. Investigations of burial diagenesis in carbonate hydrocarbon reservoir rocks. Geoscience Canada 32 (3), 103–128.

Machel, H.G. & Mountjoy, E.W. 1986. Chemistry and environments of dolomitization-a reappraisal. Earth Science Reviews 23, 175-222.

Mangione, A. 2016. Characterisation of a dolomitised offshore carbonate reservoir using basin modelling, digital rock models and high-resolution heat-flow simulations. PhD thesis, pp. 1-179, Heriot-Watt University.

Matthäi, S.K., & Heinrich, C. A. & Driesner, T. 2004, Is the Mount Isa copper deposit the product of forced brine convection in the footwall of a major reverse fault?: Geology, Vol. 32, 357–360, doi:10.1130/G20108.1.

Matthäi, S.K, Geiger, S., Roberts, S.G., Paluszny, A., Belayneh, M., Burri, A., Mezentsev, A., Lu, H., Coumou, D.,Driesner, T., & Heinrich, C.A. 2007. Numerical simulation of multi-phase fluid flow in structurally complex reservoirs. Geological Society, London, Special Publications, 292(1):405-429, doi: 10.1144/SP292.22.

Matthews A., & Katz A. 1977. Oxygen isotope fractionation during the dolomitization of calcium carbonate. Geochimica et Cosmochimica Acta, 41, 1431-1438.

McQuilken, J.1998. BG Group Internal report, 1-52.

Mejri, F., Burollet P.F. & Ben Ferjani A. 2006. Petroleum geology of Tunisia. A renewed Synthesis. ETAP Memoir N° 22 Tunis 2006.

Morrow, D.W. 1982a. Diagenesis 1. Dolomite – Part 1: The chemistry of dolomitization and dolomite precipitation. Geoscience Canada, 9, 5-13.

Morrow, D.W. 1982b. Diagenesis 2. Dolomite – Part 2: Dolomitization models and ancient dolostones. Geoscience Canada, 9, 95-107.

O'Brien, J.J., Lerche I. 1987. Heat flow and thermal maturation near salt diapirs. Dynamical Geology of Salt and Related Structures, 711-50.

Person, M., Banerjee, A., Hofstra, A., Sweetkind, D., & Gao, Y. 2008. Hydrologic models of modern and fossil geothermal systems in the Great Basin: Genetic implications for epithermal Au-Ag and Carlin-type gold deposits. Geosphere, 4(5), 888-917.

Person, M., Bense, V., Cohen, D., & Banerjee, A. (2012). Models of ice-sheet hydrogeologic interactions: a review. Geofluids, 12(1), 58-78.

Racey, A., Bailey, H.W., Beckett, D., Gallagher, L.T., Hampton M.J. & J. McQuilken. 2001. The petroleum geology of the early Eocene El Garia Formation, Hasdrubal Field, offshore Tunisia. Journal of Petroleum Geology 2001, 24, 29-53.

Saller, A.H., & Dickson, J.A.T.D. 2011. Partial dolomitization of a Pennsylvanian limestone buildup by hydrothermal fluids and its effect on reservoir quality and performance. AAPG Bullettin, 95, 10, 1745-1762.

Sclater, J.G., & Christie, P.A.F. 1980. Continental stretching: an explanation of the post-Mid-Cretaceous subsidence of the Central North Sea Basin. Journal of Geophysical Research, 85, B7., 3711-3739.

Sibson, R.H. 2007. An episode of fault-valve behaviour during compressional inversion? – The 2004 MJ6.8 Mid-Niigata Prefecture, Japan, earthquake sequence. Earth and Planetary Science Letters 257(1), 188-199.

Stanislavsky, E., & Garven, G. 2003. A theoretical model for reverse water-level fluctuations induced by transient permeability in thrust fault zones. Earth and Planetary Science Letters, 210(3), 579-586.

Sun., Q.S. 1995. Dolomite reservoirs: porosity evolution and reservoirs characteristics. AAPG Bullettin 79 No. 2, 186-206.

Vasconcelos, C., McKenzie, J.A., Warthmann R. & Bernasconi S.M. 2005. Calibration of the d18O paleothermometer for dolomite precipitated in microbial cultures and natural environments. Geology; 33;4; 317–320; doi: 10.1130/G20992.1; 2 figures; 2 tables.

Weis, P., Driesner, T., Coumou, D., & Geiger, S. 2014. Hydrothermal, multiphase convection of H2O-NaCl fluids from ambient to magmatic temperatures: a new numerical scheme and benchmarks for code comparison. Geofluids, 14(3), 347-371.

Whitaker, F.F., Smart P.L., & Jones G.D. 2004. Dolomitization: From conceptual to numerical models, in C. J. R. Braithwaite, G. Rizzi, and G. Darke, eds., The geometry and petrogenesis of dolomite hydrocarbon reservoirs:Geological Society (London) Special Publication Vol. 235, 99–139, doi 10.144/GLS.SP.2004.235.01.235.

Whitaker, F.F. & Xiao, Y. 2010. Reactive transport modelling of early burial dolomitization of carbonate platforms by geothermal convection. AAPG Bulletin, 94, no. 6, 889–917.

Wilson, M.E.J., Evans, M .J., Oxtoby, N. H., Nas, D.S., Donnelly, T. & Thirlwall M. 2007. Reservoir quality, textural evolution, and origin of fault-associated dolomites. AAPG Bulletin, 91, 1247–1272.

Wynn, T., Milne, K., 2010. Hasdrubal Field Fracture Modelling Study. AGR TRACS International Consultancy Limited, pp. 1–95.

Zaïer, A., Beji-Sassi, A., Sassi, S. & Moody, R. T. J. 1998. Basin evolution and deposition during the Early Paleogene in Tunisia. In: Petroleum Geology of North Africa (Eds D. S. MacGregor, R.t. J. Moody and D.D. Clark-Lowes). Geol. Soc. London Spec Publ., 132, 375-393.